DISSERTAÇÃO DE MESTRADO

MODELLING AND CONTROL OF WAX DEPOSITION IN SUB-SEA OIL PIPELINES

DANIEL GOMES ALBUQUERQUE

Brasília, Agosto de 2019

UNIVERSIDADE DE BRASÍLIA

FACULDADE DE TECNOLOGIA

UNIVERSIDADE DE BRASÍLIA
FACULDADE DE TECNOLOGIA
DEPARTAMENTO DE ENGENHARIA MECÂNICA

MODELLING AND CONTROL OF WAX DEPOSITION IN SUB-SEA OIL PIPELINES

DANIEL GOMES ALBUQUERQUE

DISSERTAÇÃO SUBMETIDA AO DEPARTAMENTO DE ENGENHARIA MECÂNICA DA FACULDADE DE TECNOLOGIA DA UNIVERSIDADE DE BRASÍLIA COMO PARTE DOS REQUISITOS NECESSÁRIOS PARA A OBTENÇÃO DO GRAU DE MESTRE EM SISTEMAS MECATRÔNICOS

APROVADA POR:

Prof. Dr. Eugênio L. F. Fortaleza, PPMEC/UnB
Orientador

Prof. Dr. Adriano Possebon Rosa, PCMEC/UnB
Membro Externo

Prof. Dr. Mário B. B. Siqueira, PCMEC/UnB
Membro Externo

BRASÍLIA/DF, 01 Agosto de 2019

Albuquerque, Daniel

Modelling and Control of Wax Deposition in Sub-Sea Oil Pipelines / DANIEL GOMES ALBUQUERQUE. –Brasil, 2019.

[51p.]

Orientador: Eugênio Libório Feitosa Fortaleza

Dissertação (Mestrado) – Universidade de Brasília – UnB

Faculdade de Tecnologia – FT

Programa de Pós-Graduação em Sistemas Mecatrônicos – PPMEC, 2019.

1. wax deposition 2. flow assurance 3. wax removal 4. electrical heating 5. sub-sea pipelines I. Eugênio Libório Feitosa Fortaleza, orientador. II. Universidade de Brasília. III. Faculdade de Tecnologia.

Dedicatória

Dedico este trabalho a todos que estiveram ao meu lado e contribuíram para meu crescimento pessoal e profissional. Em especial, à minha amada esposa, Lívia.

DANIEL GOMES ALBUQUERQUE

RESUMO

A deposição de parafina em linhas de produção e transporte de óleo é um dos principais problemas na área de elevação e escoamento da indústria de exploração de petróleo offshore. A perda de calor para a água fria durante o escoamento de óleos ricos em parafina através de tubulações submarinas causa a precipitação de alguns componentes de cadeia longa e sua subsequente deposição sobre as paredes internas do duto. Estes depósitos têm sua espessura incrementada com o passar do tempo, podendo ocasionar redução de vazão, aumento da potência de bombeamento e vários outros custos associados a remoção e prevenção. Neste trabalho, a taxa de deposição de parafina é predita através do cálculo de um balanço de massa na interface óleo-parafina após resolver numericamente as equações de transferência de calor e massa no interior da tubulação. A difusão molecular é considerada como o único mecanismo de deposição relevante. A remoção de parafina através do aquecimento elétrico do óleo a montante é modelada sob a hipótese de mudança de fase a temperatura constante. Este modelo é acoplado a um algoritmo de otimização visando minimizar o uso de energia elétrica. É sabido que o aquecimento da tubulação não é uma solução definitiva para o problema da parafina em linhas muito longas, devido ao fato de que a parafina dissolvida é reintroduzida no escoamento e pode eventualmente contribuir para o aumento da espessura do depósito em uma posição mais adiante. Entretanto, esta técnica permite manter a produção em níveis desejados apresentando um bom custo-benefício, especialmente em linhas de interligação poço-plataforma, em que o comprimento da tubulação torna viável a remoção integral da parafina com apenas uma estação de aquecimento, enquanto evita a necessidade de pigagem, uma alternativa consideravelmente mais cara, visto que demanda a interrupção temporária da produção.

palavras-chave: deposição de parafina, garantia de escoamento, remoção de parafina, aquecimento elétrico, dutos submarinos

ABSTRACT

Wax deposition in oil production and transportation pipelines is one of the main flow assurance problems in the offshore petroleum industry. The heat loss to the cold water environment during the flow of waxy crude oils through sub-sea pipelines causes some long-chain oil components to precipitate and deposit on the inner pipe wall. These deposits grow thicker over time, causing oil flow rate reduction, increased pumping power and several other costs associated with removal and prevention of wax deposits. In this work, the wax deposition rate is predicted through the calculation of a mass balance on the wax-oil interface after numerically solving the heat and mass transfer equations in the pipeline. Molecular diffusion is considered to be the only relevant deposition mechanism. Wax removal through electrical heating of the upstream oil is modelled under the assumption of phase change at a constant temperature. This model is coupled to an optimization algorithm for minimizing the usage of electrical energy. It is known that pipe heating is not a definitive solution to the wax problem for very long lines due to the fact that the dissolved wax is reintroduced in the oil flow and may contribute to the increase of deposit thickness further ahead. However, this technique is a cost-effective way of keeping the flow rate at a desirable level, especially in pipelines connecting oil wells to floating units, where the pipe length makes it possible to remove all wax with a single heating station, while avoiding the necessity of pigging, which is a considerably more expensive operation, since it requires a production halt.

keywords: wax deposition, flow assurance, wax removal, electrical heating, sub-sea pipelines

SUMÁRIO

LISTA DE FIGURAS

LISTA DE TABELAS

Nomenclature

Abbreviations

MWP Michigan wax predictor

PDG pressure downpipe gauge

WAT wax appearance temperature

Symbols

α thermal diffusivity (m^2/s)

$\bar{U}$ average flow velocity

Δ indicates the variation of a quantity

δ deposit thickness (m)

$\dot{q}$ heat transfer rate per unit area (W/m^2)

$\mathcal{T}$ time between heating cycles (s)

μ viscosity ($Pa.s$)

Π cost function - average cycle power (W)

ρ material density (kg/m^3)

ρ_n number density of precipitated particles (m^{-3})

ξ dimensionless radial coordinate

Bi Biot number

C concentration (kg/m^3)

C_p specific heat (J/kgK)

C_{ws} wax solubility in oil (kg/m^3)

D_{eff} effective diffusivity of wax in the deposit (m^2/s)

D_{wo} diffusivity of wax in oil (m^2/s)

E activation energy for the viscosity equation (J/mol)

E_c heating energy used per cycle (J)

f friction factor

F_w wax fraction in the deposit

h_0 overall heat transfer coefficient (W/m^2K)

k thermal conductivity (W/mK)

k_r precipitation rate (s^{-1})

P pressure (Pa)

Q oil flow rate (m^3/s)

R ideal gas constant ($8.314J/molK$)

r radial coordinate (m)

r_d deposit radius (m)

r_i internal pipe radius (m)

T temperature ($^\circ C$ or K)

t time (s)

U axial flow velocity (m/s)

x axial coordinate (m)

Chapter 1

Introduction

1.1 Context

1.1.1 Paraffin molecules in crude oil

According to Sanjay (1995) [6], "paraffin wax molecules are straight-chain alkanes that contain more than 15 carbon atoms an have very little branching." These long-chain components are less soluble in oil and have relatively high solidification temperatures. For that reason, at lower temperatures they will nucleate and precipitate out of the liquid oil to form solid wax crystals.

1.1.2 Wax formation during oil production in sub sea pipelines

During the past few decades, the oil and gas industry has turned to the offshore fields. Nowadays, nearly half of the sedimentary basins that offer good prospects of finding petroleum are located offshore[7]. With greater water depths, come the technological challenges. At depths greater than 1500m, seabed temperature will be always below 5°C. In most cases, oil production wells are located a few kilometers away from the floating unit. This means that there is a long path to be covered by the oil on seabed level before it starts to rise to the platform. In such cases, oil temperature will inevitably fall below cloud point or wax appearance temperature (WAT). When that happens, wax crystals start to precipitate in oil. This phenomenon has two undesired effects: (1) The presence of precipitated wax changes the behavior of the crude oil, usually resulting in higher effective viscosities (This can have a particularly high impact on pipeline restart[8]). (2) Wax deposition. Once the wax crystals meet the inner pipe wall, they build up a solid wax deposit. This deposit grows in thickness over time, causing the oil flow rate to drop significantly and may even block the line completely (See fig. 1.1).

An accurate prediction of the deposition rates along the pipeline is invaluable information that

Figure 1.1: Examples of wax deposition in offshore oil pipelines [1][2]

would help in the design stages of the field, as well as in the scheduling of interventions in the pipeline, in order to assure the oil flow at the desired rates[6].

Nowadays, wax deposition is the most common flow assurance problem in the petroleum industry [9]. In order to cope with wax deposit formation during oil production, interventions must be made periodically to remove wax from the pipe walls before the flow restriction becomes too prejudicial. Mechanical, thermal and chemical treatments are the three most common remediation techniques [10].

By the time this dissertation was written, very few studies were available in the literature regarding the use of electrical heating as a wax removal method. In a review article on the main mitigation and removal techniques, Al-Yaari (2011) [11] mentions electrical heating as a technique to be applied in early stages of deposition. Sarmento et. al.(2004)[12] published a work in which heating was applied through induction directly on the deposit area, as an attempt to clear a completely blocked pipe section, however the extra thermal energy introduced in the system remained mostly in the area of application. A couple of studies have assessed the use of an electromagnetic pig [13] [14] as a mobile heat source to heat up the deposit along its length.

In the current work, a different approach is proposed, in which electrical heating is applied to oil upstream from the deposit location before the flow is interrupted. This allows the heat to propagate with the flow, extending the length of actuation several kilometers beyond the location of the heating coils. This technique is a low-cost intervention, since it does not require an interruption of the oil production. On the other hand, it should demand a considerable amount of electrical power, which can be a scarce resource for an offshore production unit.

1.2 Objectives of this dissertation

1.2.1 Main objective

The goal of this work is to model the processes of deposition and removal of wax on the inner walls of a pipe, in order to develop a control strategy to optimize the use of electrical energy in the cycle of wax deposition and removal by heating.

1.2.2 Partial objectives

In order to achieve the main goal of this work, the following partial goals have been defined:

- Implement a MATLAB® code to solve the heat and mass transfer equations numerically.
- Implement a wax deposition model based on the available models in the literature
- Develop a wax removal model through the heating of upstream oil
- Develop a control strategy based on the minimization of a convex cost function

1.3 Dissertation structure

The present dissertation is organized in seven chapters, including this introduction, arranged in the following order:

Chapter 2: Deposition and Removal Mechanisms. A bibliographic review on the main deposition and mechanisms proposed by the scientific community.

Chapter 3: Mathematical Modelling. A description of the mathematical model developed to simulate wax deposition and removal in a sub-sea oil pipeline.

Chapter 4: Numerical Methods. Detailing of the numerical methods employed in the solution of partial differential equations.

Chapter 5: Optimal Control. Definition of a control strategy based on a cost function and analysis of its properties.

Chapter 6: Results and Discussion. Results of numerical simulations and discussion about their accuracy and coherence.

Chapter 7: Concluding Remarks. Main conclusions of this work and suggestions for future works.

Chapter 2

Wax Deposition and Removal Mechanisms

This chapter constitutes a review of the main deposition mechanisms proposed in the literature. Researchers such as Hunt [15], Burger et al. [16], and Leiroz and Azevedo [17] have been carrying out investigations in this area for decades. This chapter is mostly based on a critical review of wax deposition mechanisms performed by Azevedo and Teixeira [7], in which the contribution of several deposition mechanisms to the total deposition rate is evaluated. This same study also points out that shear forces may contribute to wax removal, which would affect the wax accumulation rate. Other researchers such as Nazar et al. [18] and Correra et al. [19] have considered removal mechanisms related to shear forces in their models.

2.1 Molecular diffusion

Whenever a concentration gradient occurs in a solution, a molecular diffusion mechanism will take place, attempting to reestablish homogeneity. Oil flows in sub sea pipelines are often in turbulent regime, causing the velocity, temperature and concentration profiles to be practically homogeneous along the radial coordinate, except on the vicinities of the pipe wall. For this reason, the heat and mass transfers are confined in the laminar sub-layer, where the temperature and concentration gradients are significant [7]. Since wax solubility in crude oil is an increasing function of temperature, there will be a concentration gradient as a consequence of the temperature gradient within the pipeline, with the cooler regions near the wall having the lowest wax concentration. This leads to the molecular diffusion of wax from the bulk fluid to the walls of the pipeline. Once the pipe wall temperature drops below the cloud point, wax precipitation initiates, resulting in the appearance of solid wax particles, which adhere to the wall and start to form the deposit.

The mass flux of wax can be estimated by Fick's law of diffusion as

$$\frac{dm}{dt} = -D_{wo} A \frac{dC}{dr}\bigg|_{wall}, \tag{2.1}$$

where m is the mass of parafin transported towards the wall, D_{wo} is the diffusion coefficient of wax in oil, A is the surface area over which the deposition occurs, C is the concentration of wax dissolved in oil (kg/m^3) and r is the radial coordinate.

2.2 Brownian diffusion

Brownian diffusion is a mechanism is similar to molecular diffusion, only instead of being the diffusion of liquid wax dissolved in oil, its the diffusion of precipitated wax crystals as they randomly collide with oil molecules in Brownian motion. "In the presence of a concentration gradient of solid crystals, there will be a net transport of these crystals in the direction of decreasing concentration." [7] This process can also be described by Fick's law as follows:

$$\frac{dm_b}{dt} = -D_b A \frac{dC^*}{dr}\bigg|_{wall}, \tag{2.2}$$

where m_b is the mass of wax deposited by Brownian motion, D_b is the Brownian diffusion coefficient and C^* is the concentration of solid wax crystals dispersed in oil.

The brownian diffusion mechanism has been considered negligible by several authors [15], [16], [20], but Azevedo and Teixeira [7] conclude that there is not enough experimental evidence to support that claim. Majeed et al. [21] discard Brownian diffusion as a deposition mechanism on the claim that the concentration of wax crystals is highest at the pipe wall, causing the diffusion flux to be away from the wall instead of towards it. However, because the wax crystals are trapped at the solid deposit, the concentration of free solid crystals in the liquid at the wall is nearly zero [16].

This argument can be better explained in figure 2.1, in which the continuous line represents the wax crystals concentration profile. The zero concentration boundary condition at the wall produces a peak in the concentration profile close to the wall. From this profile it can be seen that Brownian diffusion will occur in both directions from the peak and for this reason, it remains as a possible contributing mechanism for wax deposition.

2.3 Gravity settling

Wax crystals are usually denser than the oil they originated from. Therefore, gravity settling would be a possible deposition mechanism, which would contribute to the increase of the deposit thickness in the lower half of the pipeline. However, it has been classified as negligible [7], since

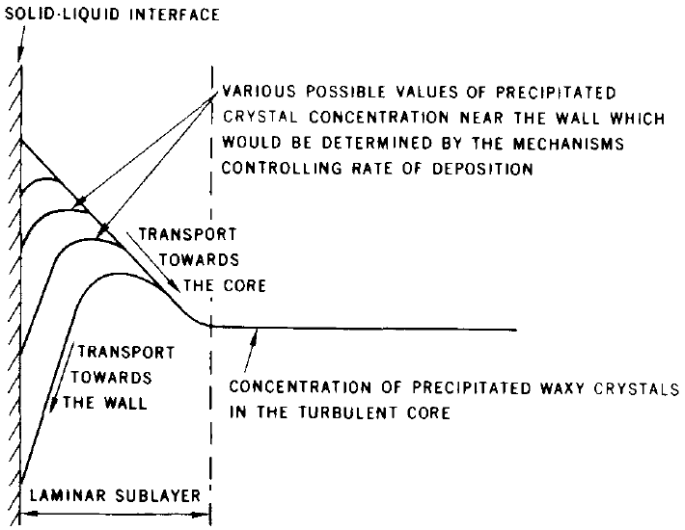

Figure 2.1: Concentration profile of precipitated solid wax (crystals) (Burger et al., 1981).

there is experimental evidence [16] showing that the settling velocities of wax crystals under typical operating conditions do not contribute significantly to the formation of wax deposits.

2.4 Shear dispersion

The shear dispersion mechanism is, as well as Brownian diffusion, a lateral transport mechanism of solid particles. Studies on concentrated suspensions reveal particle motion in the direction of reduced shear [22], [23]. This means that in the case of a pipe internal flow, shear dispersion would carry the particles away from the wall instead of towards it.

However, as Azevedo and Teixeira [7] point out, other studies have shown that particle migration occurs to a region in between the center-line and the pipe wall [24]. Wax crystals, however, present a high aspect ratio while the studies mentioned above have been carried out with spherical particles. For this reason, it is not possible to conclude that the motion observed in these experiments would be similar to that of the wax crystals.

Equation 2.3 has been proposed [16] to account for Brownian diffusion and shear dispersion, assuming that both mechanisms could be modelled by Fick's law. In this equation D_s represents the shear dispersion diffusion coefficient, which is proportional to the local shear rate. As it can be seen from equation 2.3, the flux of particles is directly proportional to a concentration gradient of solid particles and therefore the absence of deposition is expected under null heat flux conditions.

$$flux = \rho_r(D_b + D_s)\frac{dC^*}{dr}\bigg|_{wall} \tag{2.3}$$

It has been argued [7] that shear dispersion is a flow induced mechanism and therefore should

be present even in the absence of radial heat flux. However all the experiments available in the open literature show that no deposition occurs under such conditions [7]. For that reason it is concluded that shear dispersion is not a relevant mechanism for wax deposition. This statement has also been confirmed experimentally [25].

2.5 Shear stripping

Unlike the other mechanisms mentioned so far, shear stripping is a wax removal mechanism. It consists on the mechanical removal of wax crystals from the wall deposit by means of the shear tension induced by the flow on the deposit surface. The removal rate is an increasing function of wall shear rate and therefore increases as the deposit thickness becomes significant with respect to the internal diameter of the pipe. This mechanism is one of the reasons why the deposit thickness tends to stabilize at a certain plateau, especially under turbulent flow, when the shear stress is higher [26].

Matzain [27] has tried to represent this mechanism using empirical correlations for the reduction in the deposition rate caused by shear forces. An approach based on curve fitting of deposition thickness over time proposes that the removal rate is proportional to deposit thickness [26]. The experimental results have displayed very satisfactory agreement with exponential curve fittings. However, it stands on the assumption that shear removal is the only factor contributing to the stabilization of deposit thickness, when in fact there are others such as the increase of deposit surface temperature and reduction of the concentration gradient due to precipitation in the bulk [4]. An accurate model for this mechanism would help in the development of wax reducing chemicals, as some of these act by reducing the mechanical resistance of solid wax, making it more susceptible to shear stripping.

2.6 Nucleation kinetics

Many deposition models available are based on the assumption that wax precipitation kinetics does not limit the wax deposition rates. In other words, that crystal formation is practically an instant phenomenon, when observed at the time scale of wax deposition.

On a study on gelation kinetics [28], the crystallization rates of wax molecules dissolved in oil have been measured. With this study, it was demonstrated that ”nucleation represents the primary kinetic limitation associated with the crystallization of n-alkanes in organic solution at low cooling rate conditions, with crystallization rate limitations becoming significant at high cooling rates” [29].

Paso et al. [28] concludes that in pipeline systems where the bulk fluid is maintained at a tem-

perature above the fluid cloud point, nucleation may be a significant factor in the crystallization kinetics. Advancements in computational fluid dynamics of wax deposition should incorporate nucleation theory to accurately predict rates of incipient paraffin gel formation.

One of the primary limitations of current predictive deposition models is the assumption of the complete absence of kinetic limitations in the rates of incipient gel formation and deposit buildup [28]. Neglecting precipitation kinetics may ”lead to the prediction of wax deposition in cases where a stable gel cannot form” [29], resulting in unnecessary capital expenditures related to paraffin remediation and control systems. Aiyejina et al. [29] acknowledged that the results of Paso et al. [28] as well as other researches in the field of wax precipitation kinetics should prove invaluable in the development of robust wax deposition models.

Chapter 3

Mathematical Modelling

3.1 Transport equations

3.1.1 Heat Transfer

In this section the transport equations used to determine the temperature and wax concentration fields of the oil inside a cylindrical pipe are presented. By computing the heat balance in and infinitesimal annular element, like the one shown in figure 3.1, one can obtain the partial differential equation for temperature:

$$\frac{\partial T}{\partial t} = \frac{1}{r}\frac{\partial}{\partial r}\left(r\alpha\frac{\partial T}{\partial r}\right) - U(r)\frac{\partial T}{\partial x}, \tag{3.1}$$

where $U(r)$ is the velocity profile and α is the thermal diffusivity of the fluid, calculated as $\alpha = k/\rho C_p$, where k is the thermal conductivity of oil, ρ is the oil density and C_p is the oil specific heat. This equation is based on the assumption that heat diffusion in the x direction is negligible when compared to convection. Thus, the Fourier law of conduction acts solely in the radial direction, leaving the heat propagation in the axial direction entirely for convection. The velocity field is assumed to be unidirectional in the direction of x.

3.1.2 Mass transfer

To determine the wax concentration field, there can be three different approaches. The first of them is to assume that concentration of wax in the oil follows thermodynamic equilibrium with the precipitated solid wax particles[30]. This means that when the oil reaches the T_{cloud} temperature, wax molecules will precipitate and form solid particles instantly. These precipitated particles will flow with the oil and will no longer be available for deposition. That is why such hypothesis leads to an underestimation of the wax deposition rate. The concentration gradient at

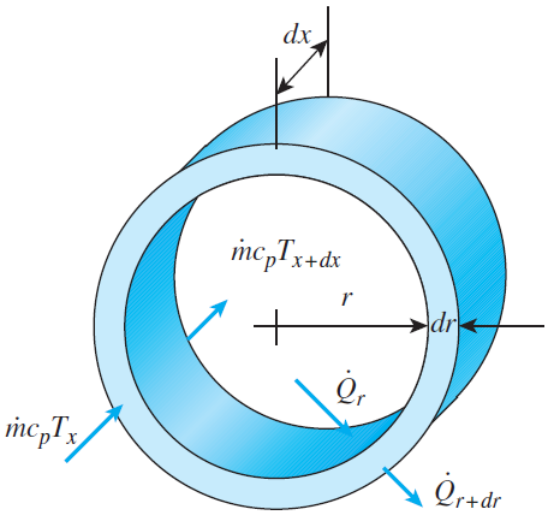

Figure 3.1: The differential volume element used in the derivation of energy balance relation.[3]

the wall (if $T < T_{cloud}$) in this situation is equal to the derivative of the solubility curve and there is no need to solve a transport equation for mass.

The second possibility is to consider that no precipitation occurs before the molecules reach either the surface of the pipe wall or the surface of the deposit[31]. This means that the heat and mass transfers are independent of each other. If this is to be considered, the equation for the concentration field can be obtained analogously to eq. 3.1, only this time performing a mass balance instead:

$$\frac{\partial C}{\partial t} = \frac{1}{r}\frac{\partial}{\partial r}\left(rD_{wo}\frac{\partial C}{\partial r}\right) - U(r)\frac{\partial C}{\partial x}. \tag{3.2}$$

Unfortunately, this assumption leads to an overestimation of the wax deposition, as more wax molecules are potentially transported to the wall via molecular diffusion [4].

As previously discussed in the last section of chapter 2, none of these assumptions are correct, since the kinetics of precipitation has to be accounted for. To solve this problem, Huang, Z.[32] has proposed a kinetic model, in which eq. 3.2 is modified with a source term:

$$\frac{\partial C}{\partial t} = \frac{1}{r}\frac{\partial}{\partial r}\left(rD_{wo}\frac{\partial C}{\partial r}\right) - U(r)\frac{\partial C}{\partial x} - k_r(C - C_{ws}(T)), \tag{3.3}$$

where C_{ws} is the solubility of wax in oil, D_{wo} is the wax difusivity in oil and k_r is the precipitation rate of wax molecules.

The wax diffusivity in oil is calculated with the correlation[33] given in equation 3.4, where μ is the oil viscosity and V_a is the molar volume.

$$D_{wo} = 13.3 \times 10^{-12} \times \frac{T^{1.47}\mu^{\gamma}}{V_a^{0.71}}, \gamma = \frac{10.2}{V_a} - 0.791. \tag{3.4}$$

The viscosity as a function of temperature is calculated with the Arrhenius equation, given in eq. 3.5, where R is the ideal gas constant and E is an activation energy specific of each substance:

$$\mu = \mu_{cloud} \exp\left[\frac{E}{R}\left(\frac{1}{T} - \frac{1}{T_{cloud}}\right)\right]. \tag{3.5}$$

An expression for k_r is given by equation

$$k_r = \frac{\pi d_n \rho_n}{2} D_{wo}(T), \tag{3.6}$$

where d_n is the diameter of the nucleus of wax particles and ρ_n is the number density of precipitated particles (m^{-3}). Although it is not possible to accurately determine these parameters, one can determine the dependence of k_r on temperature by substituting equations 3.4 and 3.5 into eq. 3.6 and taking the ratio between k_r at any temperature and k_r at the cloud point temperature. As a result of this operation, we have

$$\frac{k_r}{k_{r,cloud}} = \left(\frac{T}{T_{cloud}}\right)^{1.74} \exp\left[\frac{\gamma E}{R}\left(\frac{1}{T} - \frac{1}{T_{cloud}}\right)\right]. \tag{3.7}$$

Equation 3.7 allows one to determine the value of k_r at any temperature, with $k_{r,cloud}$ being the only unknown parameter. In their work, Huang et al.[4] have shown that a value of $k_{r,cloud} = 1.4s^{-1}$ provides simulation results that agree excellently with experimental data for various oils. Also, once should notice that since there is no precipitation of solid wax above the cloud point, the precipitation rate is null for such temperatures.

3.1.3 Stationary regime

Wax deposition is a very slow phenomenon. It may take days or even weeks for before a considerable change in thickness is perceived. For this reason, both heat and mass fields may be considered to be in stationary regime, with no prejudice to the accuracy of the solution. Mathematically, this means that the time derivatives in equations 3.1 and 3.3 can be regarded as negligible. Therefore, in order to compute both temperature and concentration fields, one needs to solve the following equations:

$$U(r)\frac{\partial T}{\partial x} = \frac{1}{r}\frac{\partial}{\partial r}\left(r\alpha\frac{\partial T}{\partial r}\right), \tag{3.8}$$

$$U(r)\frac{\partial C}{\partial x} = \frac{1}{r}\frac{\partial}{\partial r}\left(rD_{wo}\frac{\partial C}{\partial r}\right) - k_r(C - C_{ws}(T)), \tag{3.9}$$

3.1.4 Velocity Profile

Determining the real velocity profile in such complex flow demands quite a lot of modelling work. Not only is the flow in oil pipelines usually turbulent, but also the oil viscosity may display a non-newtonian behavior as a consequence of the wax content [34]. For simplicity, the flow regime considered in the transport equations described above is laminar and the velocity profile used is the quadratic profile

$$U(r) = \frac{2Q}{\pi r_d^2}\left(1 - \frac{r^2}{r_d^2}\right), \tag{3.10}$$

where Q is the volumetric oil flow rate and r_d is the deposit interface radius. The velocity profile described in equation 3.10 is assumed to preserve the quadratic shape at all times, even when the tube section is restricted by the wax deposit. This assumption is reasonable when the rate of change of the internal radius with respect to x is very low, which is the case for wax deposits.

3.2 Deposition model

Several deposition mechanisms have been suggested, including gravity settling, shear dispersion, molecular diffusion and Brownian diffusion. However, not all of them are relevant to the net deposition rate. In fact, as shown by Singh et al.[5], all deposition mechanisms are negligible except for molecular diffusion. This deposition mechanism is illustrated in Fig. 3.2, where $\mathring{i}$ is the pipe internal radius, r_d is the deposit radius and δ is the deposit thickness. Once a certain point in the oil domain reaches the wax appearance temperature(WAT), here referred to as T_{cloud}, the precipitation of solid wax crystals will occur if the local concentration of these particles is higher than the solubility limit. Precipitated particles in the bulk are carried away by the flow, while particles that precipitate on the wall will become a part of the deposit. With precipitated particles gone, the concentration of dissolved wax decreases, thus inducing a concentration gradient intimately related to the temperature field. The convective mass flux (A) is caused by the concentration gradient of dissolved wax, while the diffusive flux (B) exists due to the temperature gradient inside the deposit, since the oil trapped in it is saturated. The difference between fluxes (A) and (B) is responsible for increasing the deposit thickness, while flux (B) increases the wax fraction of the deposit. This process is known as aging[5].

Once the mass flux is obtained, one can proceed to calculate the growth and aging of the deposit over time. A mass balance at the oil-deposit interface yields the pair of coupled differential equations that describe the behavior of the deposit. Equation 3.11 is used to determine the deposition rates, while equation 3.12 gives the growth wax fraction, F_w, during the aging process. In these equations, D_{eff} is the effective diffusion coefficient of wax inside the deposit [35].

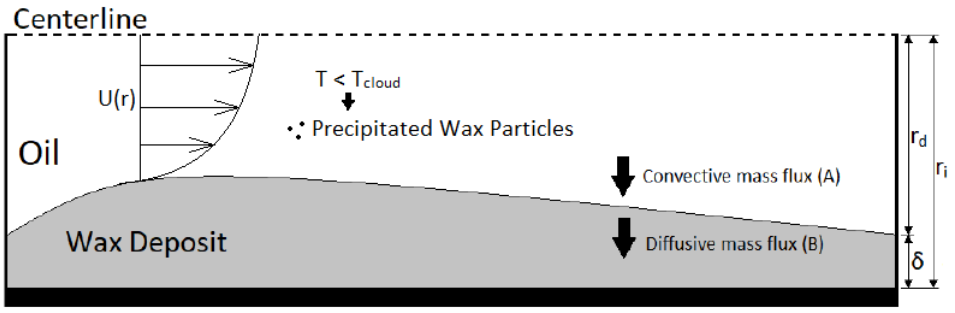

Figure 3.2: Schematics of the wax flux towards the wall and into the deposit

$$\frac{dr_d}{dt} = -\frac{1}{\rho_w F_w}\left(D_{wo}\frac{\partial C}{\partial r}\bigg|_{interface,convective} - D_{eff}\frac{\partial C}{\partial r}\bigg|_{interface,diffusive}\right), \tag{3.11}$$

$$\frac{dF_w}{dt} = \frac{2}{\rho_w(r_i^2 - r_d^2)}\left(-D_{eff}\frac{\partial C}{\partial r}\bigg|_{interface,diffusive}\right). \tag{3.12}$$

Since the oil entrapped inside the deposit is always saturated, the concentration gradient from the diffusive side can be obtained with equation 3.13, where $C_{ws}(T)$ is the wax solubility in oil. From this equation it can be observed that the solubility curve of wax in oil has a direct influence on both deposition and aging rates.

$$\frac{dC}{dr}\bigg|_{interface,convective} = \left(\frac{dC_{ws}}{dT}\right)\left(\frac{dT}{dr}\right) \tag{3.13}$$

The effective diffusion coefficient, D_{eff}, is calculated according to equation 3.14, where ϕ is the aspect ratio of the wax crystals. This formula[35] ensures that the wax fraction in the deposit is never greater than unity, as the D_{eff} approaches zero when $F_w \to 1$.

$$D_{eff} = \frac{D_{wo}}{1 + \frac{\phi^2 F_w^2}{1 - F_w}}. \tag{3.14}$$

3.3 Removal model

By heating a pipe section located upstream from the deposit location, the thermal energy is convected with the flow to the deposit region, where the wax-oil interface is heated until the surface temperature reaches T_{cloud}. Since there is no solid wax above this temperature[36], a phase changing process is initiated, during which the temperature at the interface remains constant and the difference between the heat flux from the oil to the deposit and the heat flux from the deposit to the external environment is computed as a latent heat of fusion and associated with a wax melting rate as follows:

$$\dot{m}_{melt} = \frac{\Delta\dot{Q}}{L_w} = -\frac{kA}{L_w}\frac{\partial T}{\partial r}\bigg|_{r=r_d} - \frac{h_\delta A}{L_w}(T(r_d, x) - T_\infty), \tag{3.15}$$

where L_w is the wax latent heat of fusion, A is the surface area of the deposit, h_δ is the the overall heat transfer coefficient including the thermal resistance of the wax layer, T_∞ is the undisturbed sea water temperature and $\Delta\dot{Q}$ is the difference of the heat transfer rates from the oil to the interface and from the interface to the environment. The expression for $\Delta\dot{Q}$ if valid for transient regimes when the thermal capacity of the pipe wall is neglected.

The total wax flux leaving the interface is the sum of the flux described by equation 3.15 and the diffusive flux into the deposit, illustrated in fig 3.2, responsible for the aging process. From this balance it comes that

$$\frac{dr_d}{dt} = \frac{-1}{F_w\rho_w}\left(\frac{k_w}{L_w}\frac{\partial T}{\partial r}\bigg|_{interface,convective} - \frac{h_\delta}{L_w}(T_\infty - T_{cloud}) + D_{eff}\frac{\partial C}{\partial r}\bigg|_{interface,diffusive}\right). \tag{3.16}$$

Equation 3.16 derives from the heat and mass balances at the wax-oil interface and gives the rate of change in the deposit radius during the change of phase of the deposit back into liquid wax.

In order to respect the principle of mass conservation, the flux of wax resulting from the melting at the interface has to be accounted for in the mass transfer equation. This is done through the boundary condition at $r = r_d$ and is detailed in the next section. These wax molecules reintroduced in the oil flow are driven away from the pipe wall by the same molecular diffusion mechanism that led them towards it. They are then carried away by the velocity field and may eventually form a deposit further ahead, if conditions are appropriate.

3.4 Boundary conditions

In this section the detailed boundary conditions for the transport equations are presented along with their respective associated physical hypotheses.

Since the geometry of this problem is symmetrical around the central axis of the pipe, equations 3.1 and 3.3 can be solved for $0 \leq r \leq R$ and $0 \leq x \leq L$ and the solution is valid for all planes that contain the symmetry axis. However, one may notice that these equations contain a singularity at $r = 0$. This must be addressed before we can define a boundary condition at this coordinate. The leftmost term at the right side of equations 3.1 and 3.3 can be rewritten in a general form as

$$\frac{1}{r}\frac{\partial}{\partial r}\left(r\beta\frac{\partial \Phi}{\partial r}\right) = \frac{1}{r}\frac{\partial \Phi}{\partial r}\left[\beta + r\frac{\partial \beta}{\partial r}\right] + \beta\frac{\partial^2 \Phi}{\partial r^2}, \tag{3.17}$$

where Φ represents either T or C and β represents either α or D_{wo} respectively. It is clear now that the singularity is restricted to the term $\frac{1}{r}\frac{\partial \Phi}{\partial r}$. Taking the limit of this term when $r \to 0$ and using L'hopital's rule results in

$$\lim_{r\to 0} \frac{1}{r}\frac{\partial \Phi}{\partial r} = \lim_{r\to 0} \frac{\frac{\partial}{\partial r}(\frac{\partial \Phi}{\partial r})}{\frac{\partial}{\partial r}(r)} = \frac{\partial^2 \Phi}{\partial r^2}. \tag{3.18}$$

Additionally, because of the symmetry condition, the derivative of β at $r = 0$ is null. With these results, equation 3.17 can be rewritten for $r = 0$ as

$$\frac{1}{r}\frac{\partial}{\partial r}\left(r\beta\frac{\partial \Phi}{\partial r}\right)\bigg|_{r=0} = 2\beta\frac{\partial^2 \Phi}{\partial r^2}\bigg|_{r=0}. \tag{3.19}$$

This result will be especially useful when implementing the boundary conditions numerically.

3.4.1 Heat transfer equation

The first boundary condition is the inlet temperature profile, defined at $x = 0$ for all values of r as

$$T(r, 0) = T_{inlet}. \tag{3.20}$$

At the center line, the condition of symmetry applies, yielding

$$\frac{\partial T}{\partial r}\bigg|_{r=0} = 0. \tag{3.21}$$

At the maximum radius, the oil will be exchanging heat with the external environment through the pipe walls. The heat exchange mechanism on the outside is natural convection, while inside the walls, thermal energy is transmitted through conduction. The entire thermal resistance of this system can be condensed into one combined heat transfer coefficient, as

$$h_0 = \frac{1}{r_i}\left(\frac{1}{h_e r_e} + \sum_{j=1}^{N} \frac{\ln(r_{j+1}/r_j)}{k_j}\right)^{-1}, \tag{3.22}$$

where h_e is the external natural convection coefficient, e_i are the thicknesses of material layers that separate the oil from the sea water and k_i are the respective thermal conductivities of these layers. It is important to notice that this heat transfer coefficient must be updated as the deposit grows thicker and adds an extra layer of thermal insulation between the oil and sea water. This can be done from the given initial value, h_0, by using equation 3.22 as follows:

$$h_\delta = \frac{1}{r_d}\left(\frac{1}{h_0 r_i} + \frac{\ln(r_i/r_d)}{k_d}\right)^{-1}, \tag{3.23}$$

where δ is the deposit thickness and k_d is the thermal conductivity of the deposit. The calculation of the h_δ coefficient implies permanent regime, which is the case for the wax deposition phase. During the removal phase, a transient regime is established and the temperature field should be calculated inside the pipe wall in all layers in order to accurately determine the heat transfer to the external environment. This is suggested as a future work in the last chapter.

Therefore, the boundary condition at $r = r_d$ is

$$\left.\frac{\partial T}{\partial r}\right|_{r=r_d} = -\frac{h_\delta}{k}(T(r_d, x) - T_\infty), \tag{3.24}$$

where r_d is the deposit interface radius. When $r_d = r_i$ at some x, it means that the deposit thickness is zero.

During the removal process by heating, there will still be a heat exchange between the oil and the environment. However, during this process, a phase changing phenomenon takes place when the wax-oil interface reaches the cloud point. When this happens, the boundary condition must be altered to guarantee that the temperature at the interface is no higher than T_{cloud}.

For this reason, if computing the temperature with equation 3.24 yields an interface temperature such that $T(r_d, x) > T_{cloud}$ and $r_d < r_i$, then the boundary condition is changed to

$$T(r_d, x) = T_{cloud}. \tag{3.25}$$

The last boundary condition for the heat transfer equation applies to the heated area only. The heating of the upstream oil is done with pre-installed electrical resistors arround the first few meters of pipeline. These resistors supply an evenly distributed heat source to the oil. Let $\dot{Q}$ be the total heat supply and $\dot{q} = \dot{Q}/A$ the heat transfer per unit area, the boundary condition for the heated section is given as

$$\left.\frac{\partial T}{\partial r}\right|_{r=r_i} = \frac{\dot{q}}{k}. \tag{3.26}$$

3.4.2 Mass transfer equation

Analogously to the heat transfer equation, a concentration profile is imposed at the inlet as

$$C(r, 0) = C_{inlet}. \tag{3.27}$$

Likewise, the condition of symmetry is used at the center line:

$$\left.\frac{\partial C}{\partial r}\right|_{r=0} = 0. \tag{3.28}$$

At the interface, when $r = r_d$, four different boundary conditions may apply depending on which phenomena are taking place. The first of them represents the oil in direct contact with the pipe wall, which is impenetrable by definition. For this situation, Fick's law of diffusion results in

$$\left.\frac{\partial C}{\partial r}\right|_{r=r_d} = 0. \tag{3.29}$$

Once the wall temperature reaches the cloud point, precipitation is assumed to instantly bring the concentration value to its solubility limit. In other words, when $T(r_d, x) \leq T_{cloud}$,

$$C(r_d, x) = C_{ws}(T). \tag{3.30}$$

When growing thicker, the deposit increases the thermal insulation of the oil, reducing the local heat transfer rate. Eventually this causes the interface temperature to reach the cloud point. This means that the deposit can no longer grow at that point, given that no solid wax exists above the cloud point temperature. However, a temperature gradient in the deposit is still present, as well as the saturated oil inside it. This means that the previously discussed (B) flux of wax molecules into the deposit still goes on uninterrupted (see figure 3.2).

To assure the conservation of mass of wax molecules, the same flux has to be imposed from the oil to the interface, since the deposit is now at an equilibrium state. This can be done by stating that

$$\left.\frac{\partial C}{\partial r}\right|_{r=r_d} = \frac{D_{eff}}{D_{wo}}\frac{\partial C_{ws}}{\partial T}. \tag{3.31}$$

The conditions described above are enough to simulate wax deposition. When the removal process takes place, however, another condition is necessary to ensure once more the conservation of mass. As the wax at the oil-deposit interface suffers a fusion process, the melted molecules have to be reintroduced into the oil domain. This is done by using the melted wax flux already calculated in equation 3.15 and replacing is into Fick's law equation, finally producing the last boundary condition for concentration, given as

$$\left.\frac{\partial C}{\partial r}\right|_{r=r_d} = -\frac{1}{L_w D_{wo}}\left[k\left.\frac{\partial T}{\partial r}\right|_{r=r_d} + h_\delta(T(r_d, x) - T_\infty)\right] \tag{3.32}$$

All these changes in boundary conditions during an ongoing simulation pose a numerical challenge, as the abrupt transition from one condition to another may cause quite a lot of numerical

noise. This issue will be addressed in the next chapter. Worth of notice is the fact that there is no boundary equation for $x = L$. This is only possible because the diffusion mechanism in the axial direction has been considered negligible in comparison to convection. With this assumption, the temperature and concentration values at any given location depend solely on their upstream neighbour and their own past values.

Chapter 4

Numerical Methods

In this chapter, all the methods used to solve the transport equations with their respective boundary conditions described in the last chapter are explained. The equations were solved with a finite differences algorithm with a Crank-Nicolson scheme for integration along the x direction (hyperbolic coordinate). A change in coordinates has been made in the radial direction in order to cope with the changing thickness of the deposit without having to implement an adaptive grid, and a smooth transition function has been implemented to deal with the changes in boundary conditions along the course of simulation.

4.1 Change of coordinates

From what has been exposed so far, it is already evident that the deposit radius is, in fact, a function of time and the x coordinate. This means that equations 3.1 and 3.3 would have to be solved in a variable size domain of irregular shape. To avoid dealing with such technical adversity, a change in coordinates is proposed. Taking $\xi = r/r_d$ and replacing it into the transport equations, leads to

$$\frac{\partial T}{\partial t} = \frac{1}{r_d^2 \xi}\frac{\partial}{\partial \xi}\left(\xi \alpha \frac{\partial T}{\partial \xi}\right) - U(\xi)\frac{\partial T}{\partial x}, \tag{4.1}$$

$$\frac{\partial C}{\partial t} = \frac{1}{r_d^2 \xi}\frac{\partial}{\partial \xi}\left(\xi D_{wo} \frac{\partial C}{\partial \xi}\right) - U(\xi)\frac{\partial C}{\partial x} - k_r(C - C_{ws}(T)), \tag{4.2}$$

with the velocity profile given as

$$U(\xi) = \frac{2Q}{\pi r_d^2}(1 - \xi^2). \tag{4.3}$$

The deposit radius, r_d varies only with x and t, and therefore does not affect the radial deriva-

tives. This way, the r_d^2 factor in equations 4.1 and 4.2 accounts for the variations of the deposit radius in time and space, while the PDE itself is solved numerically in a fixed rectangular grid, with $0 \leq \xi \leq 1$ and $0 \leq x \leq L$.

4.2 Finite differences

For the discretization of the governing equations, a finite differences method was used. For the radial coordinate, a central second order approximation is used to represent the derivatives in equations 4.1 and 4.2:

$$\frac{\partial}{\partial \xi}\left(\xi\beta\frac{\partial \Phi}{\partial \xi}\right) = \frac{(\xi\beta)_{i+1/2}\Phi'_{i+1/2} - (\xi\beta)_{i-1/2}\Phi'_{i-1/2}}{\Delta\xi} + \mathcal{O}(\Delta\xi^2), \tag{4.4}$$

where Φ' designates the derivative of Φ with respect to ξ in a compact notation, and the indexes $i - 1/2$ and $i + 1/2$ designate locations in the middle point between nodes. The second order approximation is used once more to express $\Phi'_{i-1/2}$ and $\Phi'_{i+1/2}$ as follows:

$$\Phi'_{i-1/2} = \frac{\Phi_i - \Phi_{i-1}}{\Delta\xi}, \tag{4.5}$$

$$\Phi'_{i+1/2} = \frac{\Phi_{i+1} - \Phi_i}{\Delta\xi}. \tag{4.6}$$

Replacing equations 4.5 and 4.6 into equation 4.4 results in

$$\frac{\partial}{\partial \xi}\left(\xi\beta\frac{\partial \Phi}{\partial \xi}\right) \approx \left[\frac{(\xi\beta)_{i-1/2}}{\Delta\xi^2}\right]\Phi_{i-1} - \left[\frac{(\xi\beta)_{i-1/2} + (\xi\beta)_{i+1/2}}{\Delta\xi^2}\right]\Phi_i + \left[\frac{(\xi\beta)_{i-1/2}}{\Delta\xi^2}\right]\Phi_{i+1}. \tag{4.7}$$

4.2.1 The Crank-Nicolson method

In numerical analysis, the Crank–Nicolson method is a second-order implicit finite difference method used for numerically solving the heat equation and similar partial differential equations. In the context of the equations solved in this work, the Crank-Nicolson method is used to integrate the transport equations along the x coordinate. This is done by writing the x derivative term as

$$\frac{\partial \Phi}{\partial x} = f\left(\xi, \beta, \frac{\partial \Phi}{\partial \xi}, \frac{\partial^2 \Phi}{\partial \xi^2}\right) \tag{4.8}$$

and then applying the trapezoidal rule with a first order approximation for the derivative

$$\frac{\partial \Phi}{\partial x} \approx \frac{\Phi_{i,j+1} - \Phi_{i,j}}{\Delta x} = \frac{1}{2}\left[f_{i,j}\left(\xi, \beta, \frac{\partial \Phi}{\partial \xi}, \frac{\partial^2 \Phi}{\partial \xi^2}\right) + f_{i,j+1}\left(\xi, \beta, \frac{\partial \Phi}{\partial \xi}, \frac{\partial^2 \Phi}{\partial \xi^2}\right)\right]. \tag{4.9}$$

The result obtained in equation 4.9 is aplied to equation 4.1. Multiplying the resulting equation by $2\xi\Delta\xi^2$ and assuming stationary regime yields the following expression:

$$\begin{aligned}\left[\frac{(\xi\alpha)_{i-1/2,j+1}}{U_{i,j+1}(r_{dj+1})^2}\right]T_{i-1,j+1} - \left[\frac{(\xi\alpha)_{i-1/2,j+1}+(\xi\alpha)_{i+1/2,j+1}}{U_{i,j+1}(r_{dj+1})^2}+\frac{\xi_i}{\varphi}\right]T_{i,j+1}+ \\ \left[\frac{(\xi\alpha)_{i-1/2,j+1}}{U_{i,j+1}(r_{dj+1})^2}\right]T_{i+1,j+1} = -\left[\frac{(\xi\alpha)_{i-1/2,j}}{U_{i,j}(r_{dj})^2}\right]T_{i-1,j}+ \\ \left[\frac{(\xi\alpha)_{i-1/2,j}+(\xi\alpha)_{i+1/2,j}}{U_{i,j}(r_{dj})^2}-\frac{\xi_i}{\varphi}\right]T_{i,j} - \left[\frac{(\xi\alpha)_{i+1/2,j}}{U_{i,j}(r_{dj})^2}\right]T_{i+1,j},\end{aligned} \tag{4.10}$$

where the i index refers to the radial coordinate, the j index refers to the x coordinate position and $\varphi = \Delta x/2\Delta\xi^2$. From equation 4.10 one can notice that this system of equations must be solved in layers, calculating the entire temperature profile at each cross section, that is, at each value of x, before going to the next one. Since the inlet profile is give, one can calculate the temperatures for $j = 2$, then for $j = 3$ and so on.

The discrete version of the mass transfer equation is very similar, with the only difference being the precipitation term. Let it be written in a compact notation as

$$\begin{aligned}[a_{i,j}]C_{i-1,j+1} + \left[b_{i,j} - k_r(T_{i,j+1})\Delta\xi^2\right]C_{i,j+1} + [c_{i,j}]C_{i+1,j+1} = \\ d_{i,j} + \left[k_r(T_{i,j})(C_{i,j} - C_{ws}(T_{i,j})) - k_r(T_{i,j+1})C_{ws}(T_{i,j+1})\right]\Delta\xi^2,\end{aligned} \tag{4.11}$$

where $a_{i,j}$, $b_{i,j}$ and $c_{i,j}$ are the exact same coefficients between brackets found on the left side of equation 4.10, only replacing α with D_{wo}. The entire right side of equation 4.10 if formed of known values, calculated in the previous iteration. This side of the equation may be condensed into one coefficient, $d_{i,j}$, which is analogous in equation 4.11.

Equations 4.10 and 4.11 represent a set of linear systems, which are solved with the Gauss elimination method for tridiagonal systems(Thomas algorithm).

4.2.2 Transient regime

Up to this point, the development of the discrete equations has been done with the assumption of stationary regime. This assumption is no longer true when the heating is turned on, as the changes in the temperature field occur at a much faster rate. Therefore, the time derivative term must be introduced. Rearranging equation 4.1 to isolate the derivative with respect to x results in

$$\frac{\partial T}{\partial x} = \frac{1}{\xi U(\xi) r_d^2}\frac{\partial}{\partial \xi}\left(\xi\alpha\frac{\partial T}{\partial \xi}\right) - \frac{1}{U(\xi)}\frac{\partial T}{\partial t}. \tag{4.12}$$

One can determine the changes in the coefficients of equation 4.10 caused by the addition of the time derivative by writing the discrete form of the time derivative in equation 4.12 is written as

$$-\frac{1}{U(\xi)}\frac{\partial T}{\partial t} = -\frac{1}{2}\left[\frac{T_{i,j}^{n+1} - T_{i,j}^{n}}{U_{i,j}^{n+1}\Delta t} + \frac{T_{i,j+1}^{n+1} - T_{i,j+1}^{n}}{U_{i,j+1}^{n+1}\Delta t}\right], \tag{4.13}$$

where the n index refers to the time coordinate.

One can then multiply equation 4.13 by $2\xi\Delta\xi^2$ and add it to equation 4.10 calculated at time $n+1$ to find out that the coefficients should be altered as follows:

$$\begin{cases} b_{i,j} \leftarrow b_{i,j} - \frac{\xi_i \Delta\xi^2}{U_{i,j+1}^{n+1}\Delta t} \\ d_{i,j} \leftarrow d_{i,j} + \frac{\xi_i \Delta\xi^2}{U_{i,j}^{n+1}\Delta t}(T_{i,j}^{n+1} - T_{i,j}^{n}) - \frac{\xi_i \Delta\xi^2}{U_{i,j+1}^{n+1}\Delta t} T_{i,j+1}^{n} \end{cases} \tag{4.14}$$

4.2.3 Boundary equations

4.2.3.1 Center Line

As discussed in chapter 3, the governing equations being solved here present a singularity in $r = 0$. For this reason, the result shown in 3.19 will be used define an equation for the center line. The differential equation to be discretized with the Crank-Nicolson algorithm at $r = 0$ is

$$U(\xi)\frac{\partial T}{\partial x} = \frac{2\alpha}{r_d^2}\frac{\partial^2 T}{\partial \xi^2}. \tag{4.15}$$

By following the same procedure as before, one arrives at the following result:

$$\begin{aligned} \left[\frac{\alpha_{1,j+1}}{U_{1,j+1}(r_{dj+1})^2}\right]T_{0,j+1} - \left[\frac{2\alpha_{1,j+1}}{U_{1,j+1}(r_{dj+1})^2} + \frac{1}{2\varphi}\right]T_{1,j+1} + \left[\frac{\alpha_{1,j+1}}{U_{1,j+1}(r_{dj+1})^2}\right]T_{2,j+1} = \\ -\frac{1}{2\varphi}T_{1,j} - \frac{\alpha_{1,j}}{U_{1,j}(r_{dj})^2}(T_{0,j} - 2T_{1,j} + T_{2,j}), \end{aligned} \tag{4.16}$$

where $i = 0$ represents a ghost node. The value for T_0 is obtained by applying the boundary condition equation. In this case, the symmetry condition is applied, which is equivalent to stating that $T_0 = T_2$ in a second order approximation of the radial derivative. As a result, the following equation is obtained:

$$-\left[\frac{2\alpha_{1,j+1}}{U_{1,j+1}(r_{dj+1})^2} + \frac{1}{2\varphi}\right]T_{1,j+1} + \left[\frac{2\alpha_{1,j+1}}{U_{1,j+1}(r_{dj+1})^2}\right]T_{2,j+1} = -\frac{1}{2\varphi}T_{1,j} - \frac{2\alpha_{1,j}}{U_{1,j}(r_{dj})^2}(T_{2,j} - T_{1,j}). \tag{4.17}$$

Once again the mass transfer equation is analogous except for the precipitation term. It and can be written as

$$\begin{aligned}\left[b_{i,j} - \frac{k_r(T_{1,j+1})}{2}\Delta\xi^2\right]C_{1,j+1} + [c_{i,j}]C_{2,j+1} = \\ d_{i,j} + \left[\frac{k_r(T_{1,j})}{2}(C_{i,j} - C_{ws}(T_{i,j})) - \frac{k_r(T_{1,j+1})}{2}C_{ws}(T_{i,j+1})\right]\Delta\xi^2.\end{aligned} \tag{4.18}$$

4.2.3.2 Wall or deposit interface

The boundary condition at $r = r_d$ is applied directly, by replacing the last equation of the system with the discrete version of equation 3.24 as follows:

$$\frac{T_{N,j+1} - T_{N-1,j+1}}{r_{dj+1}\Delta\xi} = -\frac{h_{\delta,j+1}}{k}(T_{N,j+1} - T_\infty), \tag{4.19}$$

where $i = N$ is the last radial position.

Although this first order expression introduces a bigger approximation error, this approach has been chosen as an alternative to avoid the numerical noise that resulted from applying the boundary condition directly to the governing equation. Reorganizing equation 4.19 yields

$$-T_{N-1,j+1} + \left[1 + \Delta\xi Bi_{j+1}\right]T_{N,j+1} = \Delta\xi Bi_{j+1}T_\infty, \tag{4.20}$$

where $Bi = h_\delta r_d/k$ is the Biot number.

The same procedure applies for the mass transfer equation with its four different boundary conditions at the interface.

4.3 Boundary condition transitions

The abrupt transition between boundary conditions in an ongoing simulation causes a considerable level of numerical noise in the solution. One way to overcome this problem is to make the transition gradually with a smoothing function. The chosen function was the following:

$$H(p) = \begin{cases} 0 & \text{if } p < -\varepsilon \\ \frac{1}{2}\left[1 + sin\left(\frac{\pi}{2} - \pi\frac{p}{\varepsilon}\right)\right] & \text{if } -\varepsilon \le p \le 0\ , \\ 1 & \text{if } p > 0 \end{cases} \tag{4.21}$$

where ε is the size of the transition interval and p is the transition parameter. With this definition, function $H(p)$ makes a smooth transition from 0 to 1 with a continuous first derivative.

Fortunately, the diffusion coefficient of the mass transfer equation is small enough to allow instant transitions without generating numerical noise. For the heat transfer equations, however, this is not the case.

The general form of the boundary equation at $\xi = 1$ is

$$a_{N,j+1}T_{N-1,j+1} + b_{N,j+1}T_{N,j+1} = d_{N,j+1} \tag{4.22}$$

As it will be detailed in the following sections, the a_N, b_N and d_N are modified according to the boundary condition applied. The smooth transition is assured by the $H(p)$ function.

4.3.1 Upstream heating

Once the deposit has grown to a certain size considered critical for the operation of oil production, the pipe heating is turned on. Along the heated section of the pipe, the direction of heat flux is inverted as the oil starts to gain energy from the walls instead of losing it to them. Looking at the boundary equation for $r = r_d$, one can see that this transition can be executed by a change in coefficients as

$$\begin{cases} a_N = -1 \\ b_N = 1 + \Delta\xi Bi_{j+1} \\ d_N = \Delta\xi Bi_{j+1}T_\infty \end{cases} \longrightarrow \begin{cases} a_N = -1 \\ b_N = 1 \\ d_N = \frac{\dot{q}r_d\Delta\xi}{k} \end{cases} . \tag{4.23}$$

This transition can be done with function $H(p)$ described in equation 4.21. I this particular case, the transition parameter is time. The resulting expression for the coefficients is

$$\begin{cases} a_N = -1 \\ b_N = 1 + \Delta\xi Bi_{j+1}[1 - H(t - t_s)] \\ d_N = \Delta\xi Bi_{j+1}T_\infty[1 - H(t - t_s)] + \frac{\dot{q}r_d\Delta\xi}{k}H(t - t_s) \end{cases} , \tag{4.24}$$

where t_s is the time at which the heating resistors are switched on.

4.3.2 Phase change at a constant temperature

The hot oil take a while to reach the deposit region, and when it does, the wax-oil interface temperature will rise until it reaches the cloud point temperature. At this temperature, a phase change is initiated, resulting in a thickness reduction. In order to assure that this process occurs at a constant temperature, the boundary condition equation is changed from equation 4.20 to $T_N = T_{cloud}$. The changes in coefficients are:

$$\begin{cases} a_N = -1 \\ b_N = 1 + \Delta\xi Bi_{j+1} \\ d_N = \Delta\xi Bi_{j+1} T_\infty \end{cases} \longrightarrow \begin{cases} a_N = 0 \\ b_N = 1 \\ d_N = T_{cloud} \end{cases} . \tag{4.25}$$

One can use function $H(x)$ described in equation 4.21 to make this transition smoothly by writing

$$\begin{cases} a_N = -1 + H(x - x_d) \\ b_N = 1 + \Delta\xi Bi_{j+1}[1 - H(x - x_d)] \\ d_N = \Delta\xi Bi_{j+1} T_\infty [1 - H(x - x_d)] + T_{cloud} H(x - x_d) \end{cases} . \tag{4.26}$$

Chapter 5

Optimal Control

In this chapter, a first attempt to minimize the electrical energy used in wax removal is presented. An objective function has been defined and used to determine the duration and periodicity of the heating phase.

5.1 The Cost Function

In mathematical optimization, a loss function or cost function is a function that maps an event or values of one or more variables onto a real number intuitively representing some ”cost” associated with the event. An optimization problem seeks to minimize a cost function.

In the context of wax deposition in sub-sea pipelines, wax removal is a procedure that must be executed periodically to ensure the continuity of the oil production at desirable levels. Minimizing the electrical energy demand for the removal operation is equivalent to minimizing the mean electrical power, calculated as

$$\Pi(t) = \frac{E_c(t)}{\mathcal{T}(t)}, \tag{5.1}$$

where E_c is the total electrical energy spent on removal and $\mathcal{T}$ is the period between consecutive removal interventions, given that the heating duration is t seconds. Given that the heating instant power, P, is a constant value, $E_c(t)$ is simply Pt, where t is the period of time during which the resistors are active.

On the other hand, estimating the value of $\mathcal{T}$ requires a more elaborate procedure, involving the calculation of the pressure drop across the pipeline. These calculations shall be considered in the next subsection.

5.1.1 Pressure Drop in a Horizontal Pipe

The transportation of a fluid in a pipeline is driven by a pressure difference across it. This pressure gradient is necessary to overcome the internal dissipative forces in the fluid associated with the shear rate induced by the flow. The pressure gradient in a horizontal pipeline is calculated as

$$\frac{dP}{dx} = \frac{f}{D}\frac{\rho\bar{U}^2}{2}, \tag{5.2}$$

where f is the friction factor, ρ is the density of the fluid, $\bar{U}$ is the average profile velocity and D is the internal diameter of the pipe. For laminar flow regimes, the friction factor is given as a function of the Reynolds number as $f = 64/Re$. The Reynolds number is calculated as

$$Re = \frac{\rho\bar{U}D}{\mu} = \frac{2\rho Q}{\mu\pi r_d}, \tag{5.3}$$

where μ is the viscosity of the fluid and Q is the volumetric flow rate. The combination of equations 5.2 and 5.3 with the expression for the friction factor in laminar flows yields the following expression for the pressure gradient:

$$\frac{dP}{dx} = \frac{8\mu Q}{\pi r_d^4}. \tag{5.4}$$

In order to obtain the pressure difference across the pipeline, one should integrate equation 5.4 along the pipe length (L):

$$\Delta P = \frac{8\mu Q}{\pi}\int_0^L r_d^{-4}(x)dx. \tag{5.5}$$

5.1.2 Estimation of the $\mathcal{T}$ parameter

The time history of ΔP during the deposition phase is recorded in order to allow the calculation of $\hat{\mathcal{T}}$, which is the estimated value of $\mathcal{T}$. Figure 5.1 shows both $\mathcal{T}$ and its estimated value, $\hat{\mathcal{T}}$. Given an instant value of the pressure drop during the removal phase, $\hat{\mathcal{T}}$ is the time interval between the present time and the last time ΔP had the same value. One might think, by looking at figure 5.1, that the wax removal happens in no time, but it actually takes a few hours. However, considering a time scale of two months, it is indeed practically instantaneous.

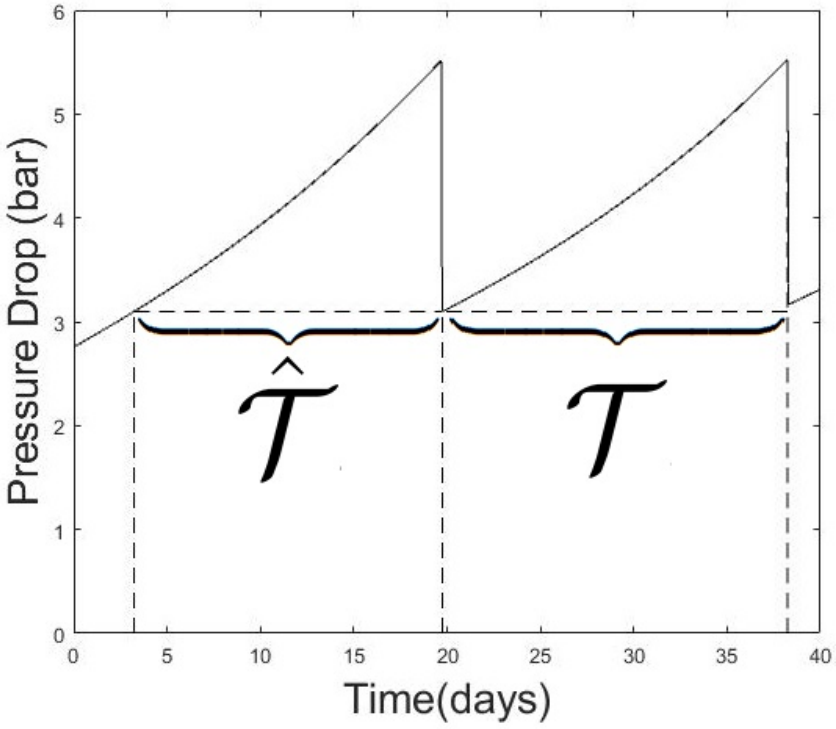

Figure 5.1: An illustration of how the $\hat{\mathcal{T}}$ parameter is calculated

5.2 Aspects of the Π function

In this section, a few aspects of the Average Cycle Power (Π) are analyzed. In order to do so, it is necessary to physically understand what happens when the heating resistors are turned on. Since the deposit section starts a few hundred meters (or maybe a few kilometers) ahead of the inlet position, it takes a certain amount of time for the hot oil to reach the deposit. This lag period shall be called t_{lag}. During this period, the $\mathcal{T}$ parameter is equal to heating duration, τ, and therefore, we have

$$\Pi(t) = P \text{ , if } t < t_{lag} \tag{5.6}$$

After the wax removal starts, the $\mathcal{T}$ parameter starts to rapidly increase, as it can be inferred from figure 5.1, a small decrease in ΔP causes a huge increase in $\mathcal{T}$ due to the derivative of the curve. This causes an abrupt reduction of the Π function.

After the removal phase is over, whether the wax has been completely removed or not, the derivative of $\mathcal{T}$ with respect to time becomes 1, since ΔP remains constant. The limit of $\Pi(t)$ when t approaches infinity, by L'hôpital's rule is

$$\lim_{t\to\infty} \Pi(t) = \lim_{t\to\infty} \frac{E_c}{\mathcal{T}} = \lim_{t\to\infty} \frac{dE_c}{dt}\left(\frac{d\mathcal{T}}{dt}\right)^{-1} = P. \tag{5.7}$$

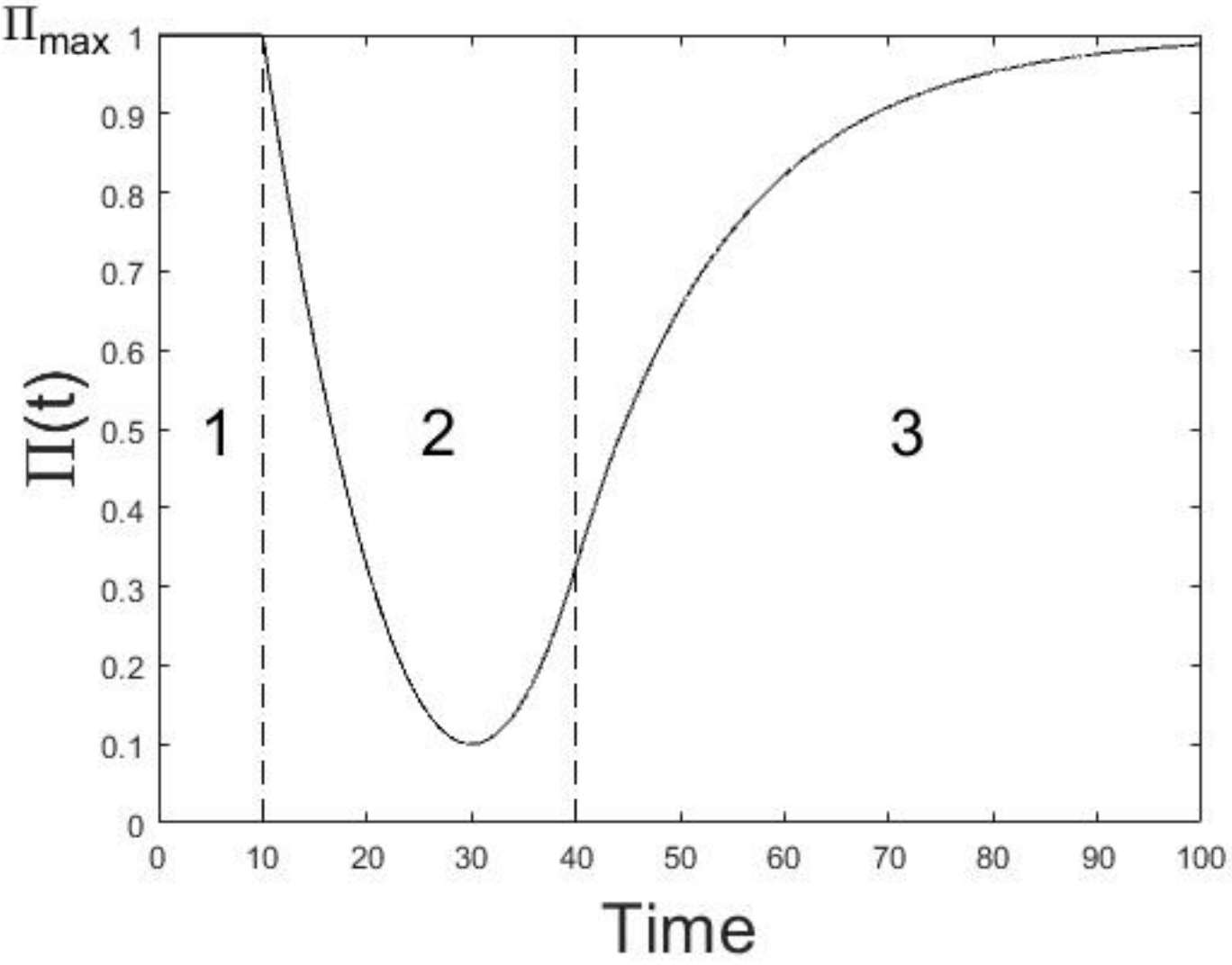

Figure 5.2: Typical $\Pi(t)$ curve

From these aspects of the Π function one must conclude that there has to be a minimum value of $\Pi(t)$ for $t > t_{lag}$. The typical behavior of the cost function with a continuously active heating is shown in figure 5.2. This curve can be divided in three sections. Section 1 represents the energy expenditure with zero wax removal, because the hot oil has not yet reached the solid wax (lag period). Section 2 starts as soon as the wax begins to change phase, resulting in a thickness reduction of the deposit. In this section, the Π function is convex, and a minimum value can be found. Section 3 starts at the point of inflection, when the Π starts to exhibit an asymptotic behavior towards its maximum value, P, which is the instant heating power.

Chapter 6

Results and Discussion

This chapter is dedicated to the verification, validation and discussion of the numerical results obtained from the models described in the previous chapters.

All the simulation results displayed in this chapter have been obtained with the discretization parameters shown in table 6.1.

Table 6.1: Mesh parameters

Mesh Property	Unit	Value
Number of nodes in ξ direction	$-$	100
$\Delta\xi$	$-$	0.01
Number of nodes in x direction	$-$	1001
Δx	m	2
Total number of nodes	$-$	100.100
Maximum time step for deposition phase	h	10
Maximum time step for removal phase	s	1

6.1 Verification

6.1.1 Heat Transfer Model

The first method chosen do verify the heat transfer simulation is by imposing a constant heat flux per unit area at the wall. This boundary condition is described mathematically as

$$-k\frac{\partial T}{\partial r}\bigg|_{r=r_i} = \dot{q}, \tag{6.1}$$

where $\dot{q}$ is given in watts per square meter.

In such conditions, the oil temperature profile along ξ should develop from a uniform profile into a fourth order function of ξ, given as

$$T(\xi, x) = T(1, x) + \frac{\dot{q}r_i}{k}\left(\frac{3}{4} - \xi^2 + \frac{1}{4}\xi^4\right), \tag{6.2}$$

where $T(1, x)$ is the surface temperature at the pipe wall. This equation can be rearranged for comparison purposes as

$$T(\xi) - T(1, x) = \frac{\dot{q}r_i}{k}\left(\frac{3}{4} - \xi^2 + \frac{1}{4}\xi^4\right). \tag{6.3}$$

As one can see, the right hand side of equation 6.3 is independent of x. This allows for comparison between profiles at any given x. As long as the temperature profile is fully developed, the function $T(\xi, x) - T(1, x)$ should be the same. This can be observed to be true in figure 6.1 below:

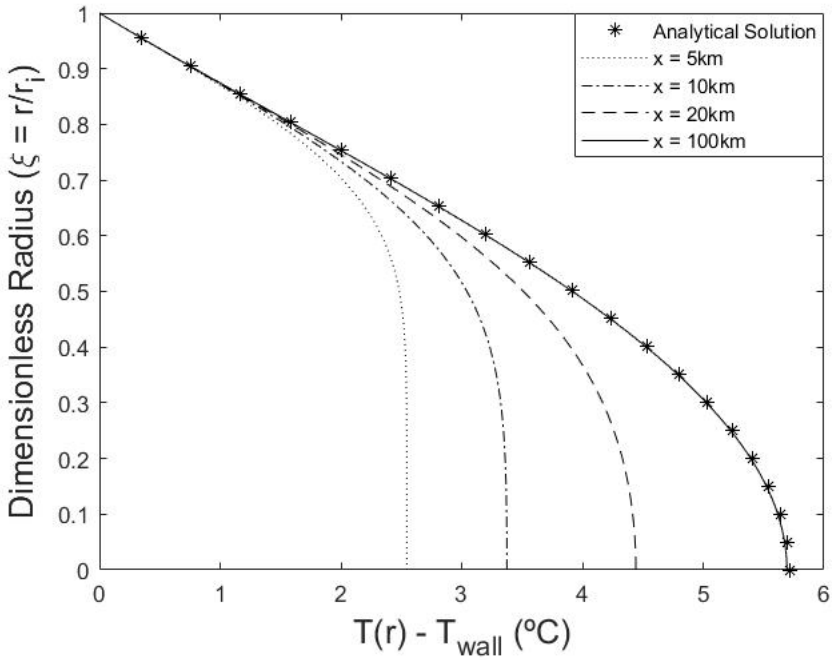

Figure 6.1: Development of the simulated temperature profile in agreement with the analytical solution

A direct consequence of the result displayed in figure 6.1 is that, since the profile of temperature differences remains constant along x, the temperature gradients along this coordinate must be the same for every value of ξ. This can be verified with the result shown in figure 6.2, where

the temperature curves become parallel after a certain value of x, known as the thermal boundary layer development length.

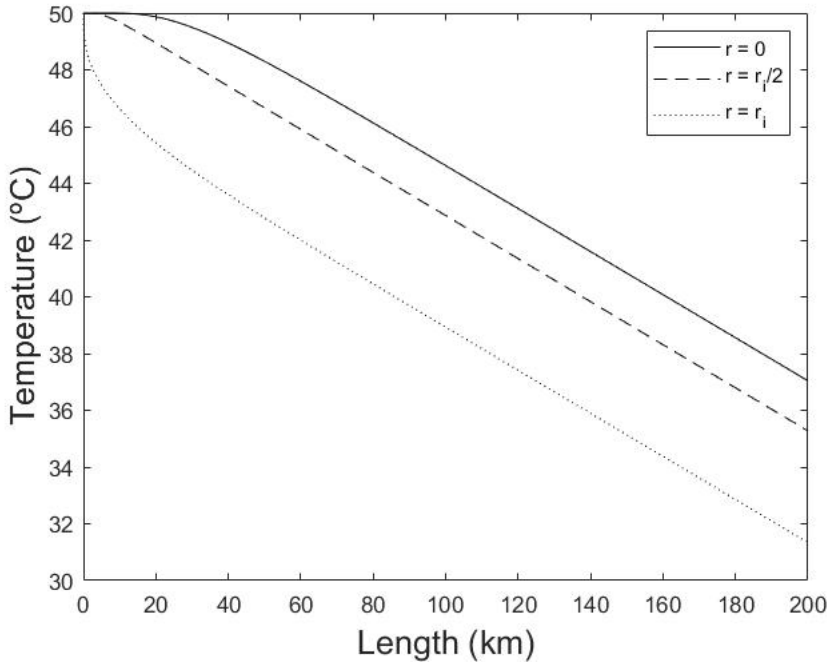

Figure 6.2: Temperature for different values of r along the entire pipeline

The analytical solution for the temperature field with a prescribed heat flux at the wall also allows for the calculation of the axial derivative of temperature, given as

$$\frac{\partial T}{\partial x} = -\frac{2\dot{q}}{\rho \bar{U} C r_i}, \tag{6.4}$$

where $\bar{U}$ is the mean value of the velocity profile. Figure 6.3 shows the numerical results in agreement with equation 6.4.

The last validation test analyses the behavior of the average bulk temperature as function of the heat flux at the wall. The average bulk temperature is calculated by assuming a homogeneous temperature profile that would transport the same amount of thermal energy as the actual profile. Therefore, it is calculated as

$$T_{bulk} = \frac{2}{\bar{U} r_i^2} \int_0^{r_i} T(r) U(r) r dr, \tag{6.5}$$

where $\bar{U}$ is the average flux velocity.

To perform the following test, the global heat transfer coefficient was set to zero for $x > L/2$. More specifically, in a 200km pipeline, there will be no heat transfer after the mark of 100 kilometers. The result of this simulation is shown in figure 6.4, where it can be seen that all the

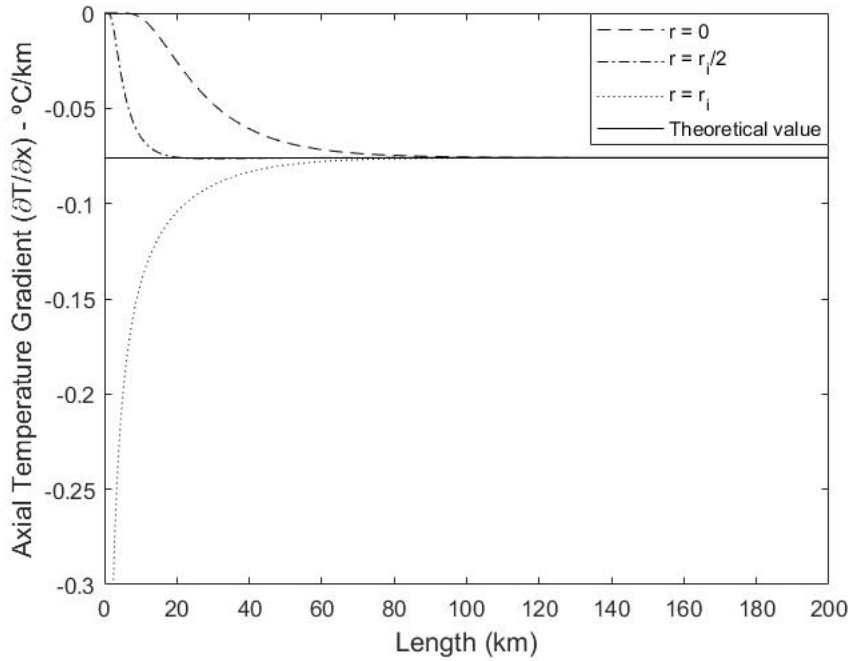

Figure 6.3: Axial temperature gradient for different values of r along the pipeline

temperature values converge to the bulk temperature in the absence of external heat flux, generating an uniform temperature profile. Additionally, it can be observed that the bulk temperature maintains a constant value from the insulation point onward, which is expected, since there is no change in internal energy. This result also calls the attention to an interesting fact: A reduction in the heat transfer coefficient will cause an increase in the wall temperature. This effect will be present in the full simulation, where the deposition of wax creates an insulation layer, causing the interface temperature to rise.

This concludes the verification of the heat transfer model.

6.1.2 Mass Transfer Model

The mass transfer model is verified with analogous tests, since the equations are mathematically equivalent to each other, apart from the precipitation term. The first validation method is to prescribe a mass flux per unit area at the wall and check the concentration profile. The boundary condition utilized for this purpose is

$$-D\frac{\partial C}{\partial r} = \dot{m}, \tag{6.6}$$

where $\dot{m}$ is the specified mass flux per unit area, given in $kg.s^{-1}.m^{-2}$. The analytical fully developed concentration profile for this problem is

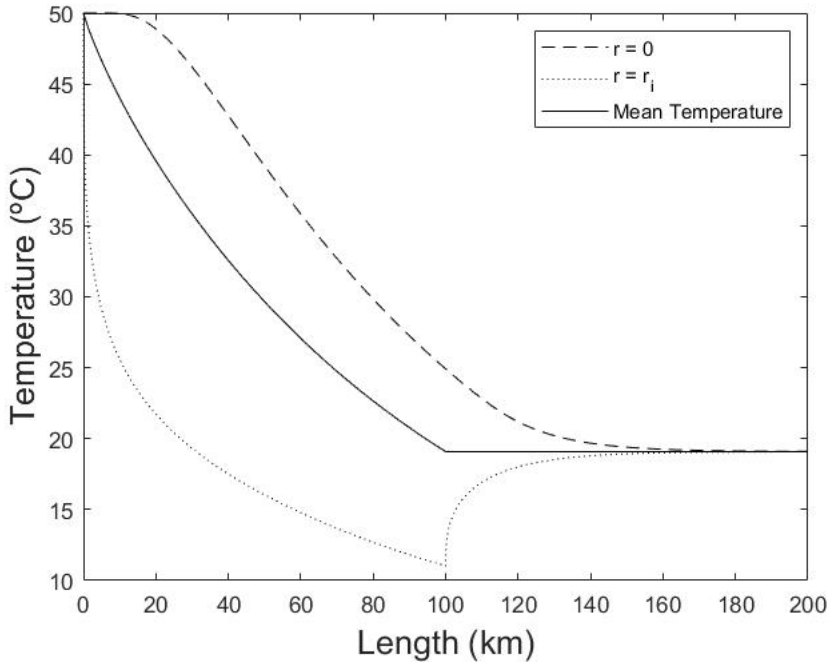

Figure 6.4: Average bulk temperature, center line temperature and wall temperature for a pipeline with perfect insulation in half of its length

$$C(\xi, x) = C(1, x) + \frac{\dot{m} r_i}{D_{wo}} \left(\frac{3}{4} - \xi^2 + \frac{1}{4}\xi^4 \right), \tag{6.7}$$

where it can be noted that the difference between the concentration at a given ξ and the concentration at the wall ($\xi = 1$) for the same value of x is not a function of x. This allows for comparison between concentration profiles in several different sections of the pipeline, as it can be seen in figure 6.5. To perform this test, the wax-in-oil diffusivity had to be altered so that the development length of the concentration profile would fit in the pipe length.

The next step of validation is to verify that the axial concentration gradients converge to the same value after the profile is stabilized. In figure 6.6 it can be noticed that the concentration curves become parallel, indicating that all of them present the same change rate with respect to x.

Furthermore, the slopes of the curves shown in figure 6.6 may be compared to the analytical solution, which is given as

$$\frac{\partial C}{\partial x} = \frac{2\dot{m}}{\bar{U} r_i}. \tag{6.8}$$

This comparison is shown in figure 6.7, where it can be observed that all curves converge to the analytical solution described by equation 6.8.

The last test is to verify the behavior of the average bulk concentration as a function of the mass flux at the wall. For this purpose, the condition of impermeability has been imposed at the

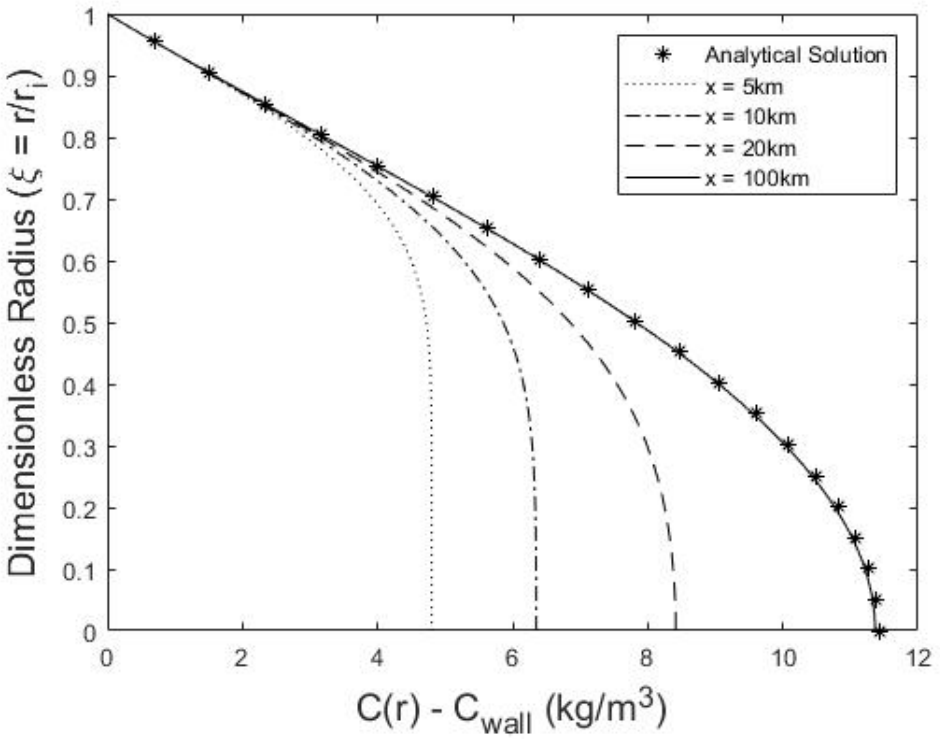

Figure 6.5: Development of the simulated concentration profile in agreement with the analytical solution.

last half of the pipe. The consequences of this condition in the concentration curves along the x coordinate can be observed in figure 6.8, where all the concentration values converge to the average bulk concentration after the mass flux is interrupted. Additionally, it can be seen that the bulk concentration remains constant along the entire second half of the pipe, as it is expected since there is no mass flux in this section. This concludes the verification of the mass transfer model.

6.1.3 Deposition Model

This subsection is dedicated to validating the wax deposition model, which comprises the heat and mass transfer models as well as the deposition and aging equations. Ideally, such validation should be done through comparison with experimental data. However, by the time this dissertation was elaborated, no complete set of parameters have been found in the literature that would allow to set up a simulation that would represent a specific experiment. Therefore, the following comparisons are of qualitative nature only.

The wax deposit thickness as a function of time displays a behavior resembling an exponential function. After some time, it stabilizes at a maximum value. This occurs mainly because, as the interface temperature rises, so does the solubility limit, which is the concentration value at the

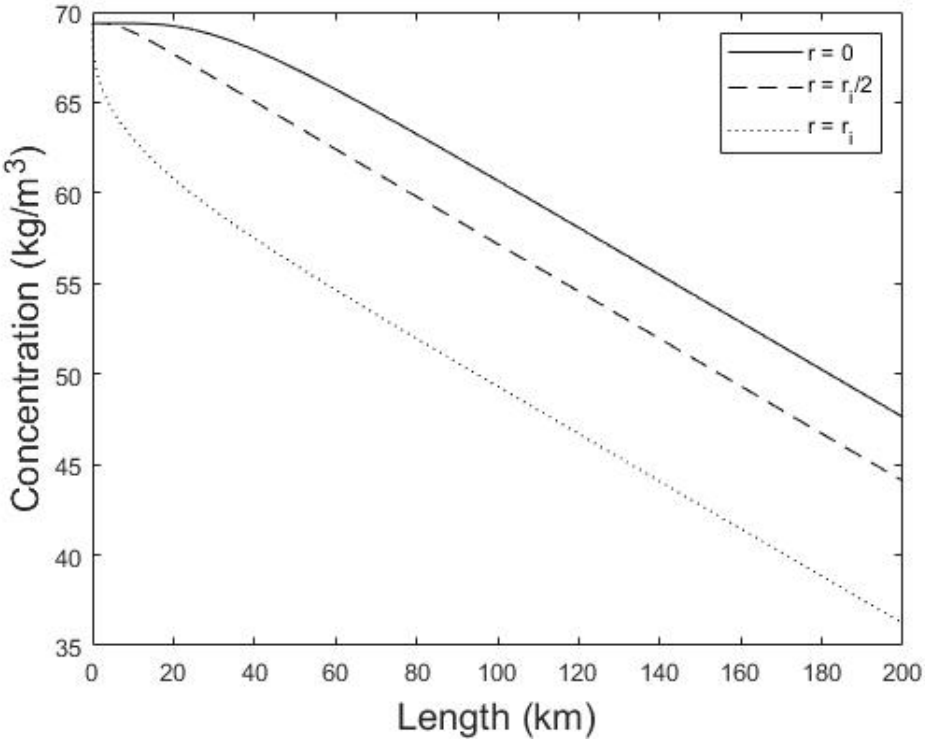

Figure 6.6: Wax Concentration for different values of r along the pipeline.

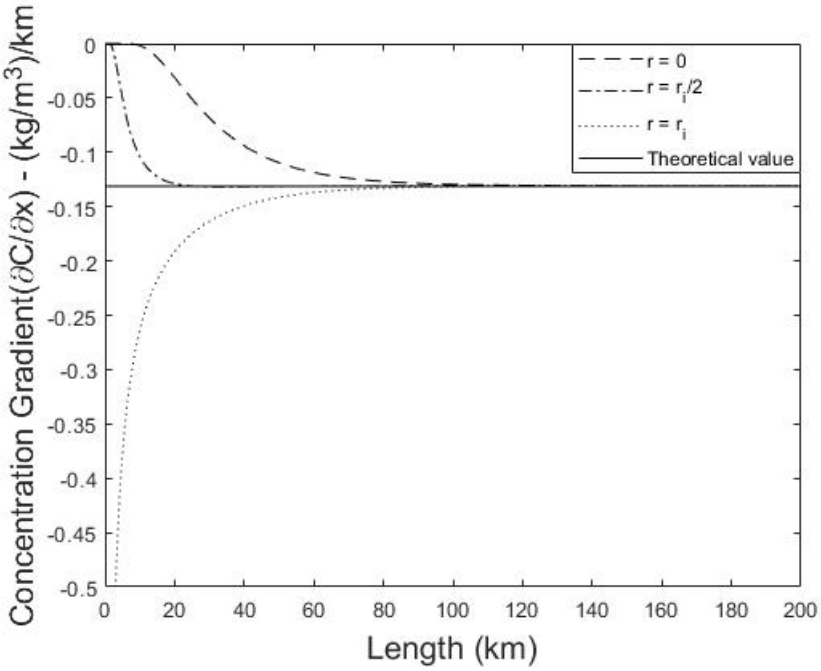

Figure 6.7: Axial wax concentration temperature gradient for different values of r along the pipeline.

interface. This reduces the concentration difference between the interface and the bulk. When this difference is null, there is no driving force to transport wax molecules towards the wall and

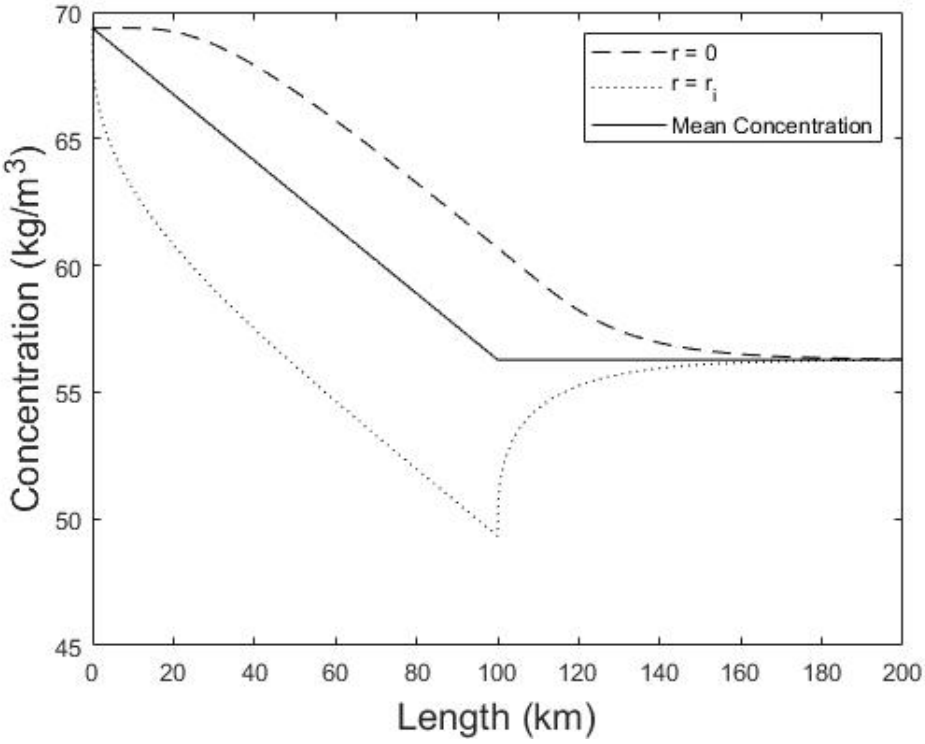

Figure 6.8: Average bulk concentration, center line concentration and wall concentration for a pipeline with impermeable walls on the second half of its length.

therefore the deposition ceases.

Such behavior can be verified both experimentally and numerically. Figure 6.9 shows the comparison of two deposition experiments with the current work. The time variable has been made non dimensional with the τ parameter, which is the characteristic time of the fitting exponential function for each data set.

The shape of the axial thickness profile may vary considerably from one oil to another. Several oil properties have an influence on this profile, such as the cloud point temperature, thermal conductivity, viscosity etc. One of the most influential characteristics is the solubility curve, $C_{ws}(T)$, as it dictates the axial concentration profile on the wall as well as the wax flux into the deposit(see equation 3.13). Figure 6.10b shows different shapes of axial thickness profiles for different oils obtained in the work of [4]. On the left hand side, figure 6.10a exhibits an axial wax thickness profile obtained in this work.

All these different profiles can be divided into three different sections: (1) region with no deposition, since the cloud point temperature has not yet been reached, (2) peak deposition rates, and (3) reduced deposition. As the fluid enters the second section, where the inner wall temperature is below T_{cloud}, molecules start to deposit on the wall, resulting in significant wax build up in this section. In the third section, the bulk temperature of the oil has decreased significantly and is close to the ocean temperature. This causes a reduction in the radial thermal gradient in the oil,

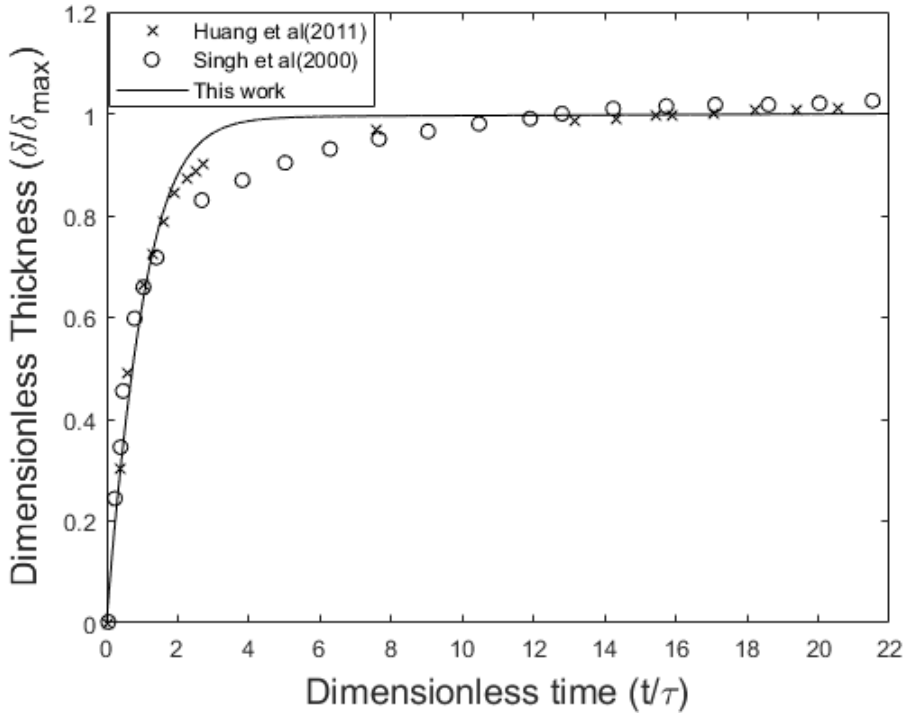

Figure 6.9: Deposit thickness as a function of time. Comparison with experimental data [4][5]

that leads to a decrease in the driving force of deposition ($C_{bulk} - C_{interface}$).

6.2 Wax Deposition in a Well-to-Platform Pipeline

Pipelines connecting production wells to platforms ar usually only a few kilometers long. These lines also suffer with wax deposition, but their short length in comparison to oil exportation lines is a big advantage when it comes to wax removal through heating. In the following simulation, a two kilometer pipeline with an internal diameter of 6 inches is simulated with heating applied to the first two hundred meters from inlet position during removal phase.

The length and diameter of this pipeline represent typical dimensions of a sub-sea well-to-platform pipeline. Table 6.2 summarizes the input data used in the simulation, based on typical values for oil properties and pipeline dimensions. It is important to note that although the Reynolds number characterizes a flow in the laminar-turbulent transition, this model considers a completely laminar regime. Turbulence shall be included in future works.

Figure 6.11 shows the concentration field along the pipeline. Due to the order of magnitude of the diffusion coefficient, which is of $10^{-10}m^2/s$, the significant values of concentration gradient due to wall precipitation are all confined in a very thin boundary layer with a maximum thickness approximately 3% of the pipe radius. The radial gradient starts at 300m from the inlet, where the wall temperature reaches the cloud point, and extends to the end of the pipeline.

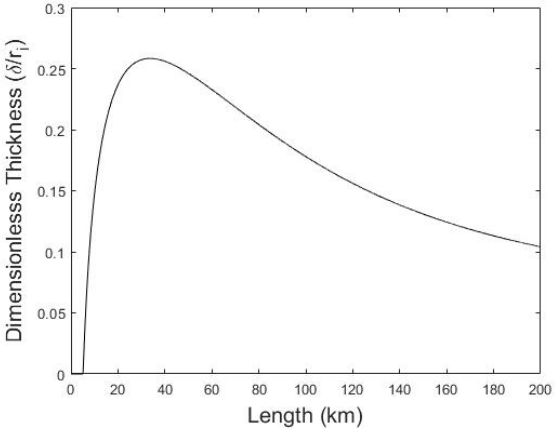

(a) Axial thickness profile after 50 days of deposition(this work)

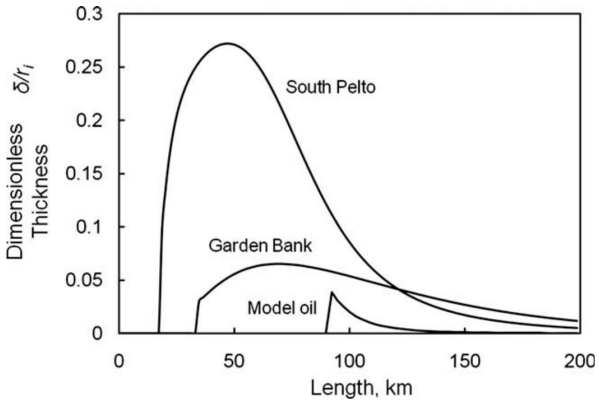

(b) Axial thickness profiles for oils with different properties[4]

Figure 6.10: Axial thickness profile comparison

Table 6.2: Oil properties used in simulation

Oil Property	Unit	Value
Cloud point temperature	$°C$	40
Inlet temperature	$°C$	50
External temperature	$°C$	4
Overall heat transfer coefficient	W/m^2K	3
Wax content	$\%$	8.5
Viscosity at T_{cloud}	$mPa.s$	50
Specific mass	kg/m^3	750
Flow rate	m^3/s	3.65×10^{-2}
Reynolds number	-	4574
Specific heat	J/kgK	2300
Latent heat	J/kg	23000
Thermal conductivity	W/mK	0.1

The deposition profiles along the axial direction are shown in figure 6.12a for three different periods of time. The solid line represents the maximum possible size of the deposit, as the interface temperature has reached the cloud point, above which there can be no solid wax. Since the wax content of this oil is higher than the solubility limit at T_{cloud}, the surface temperature limit is the only mechanism that keeps the deposit from growing further. On the right hand side, figure

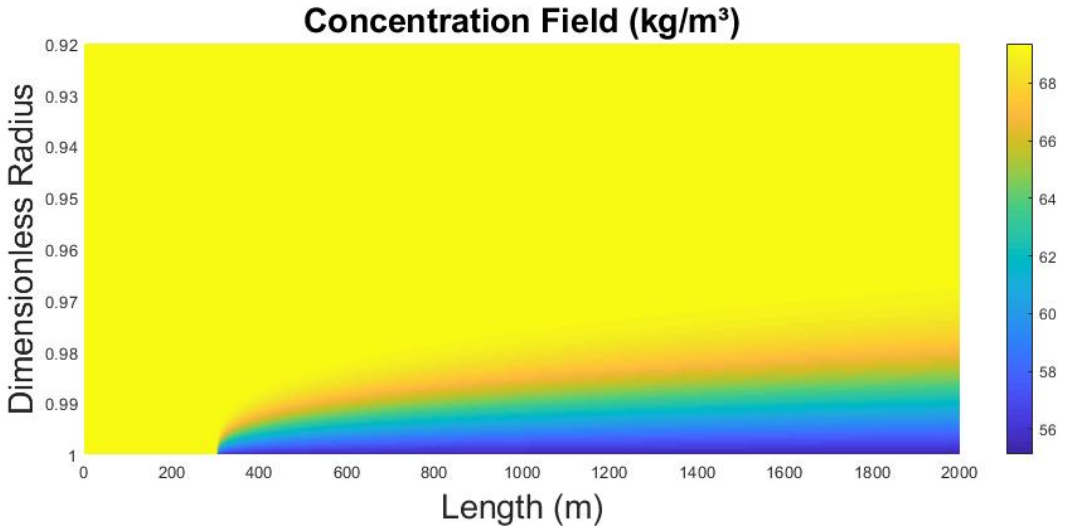

Figure 6.11: Concentration field near the wall

6.12b shows the interface temperature change as the deposit becomes thicker.

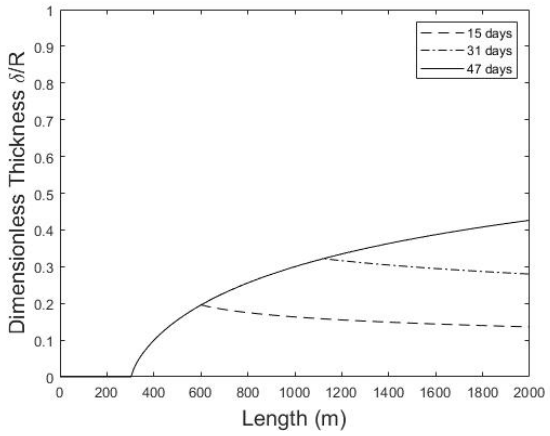

(a) Predictions of the wax deposit thickness profile for different periods of time.

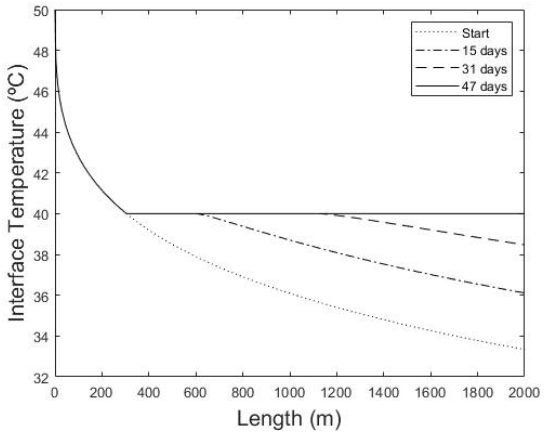

(b) Interface temperature profile for different periods of time.

Figure 6.12: Time progression of wax deposition over 47 days

Although the wax deposition has ceased, the aging process goes on uninterrupted, as it can be seen in figure 6.13. The wax fraction of the deposit is directly related to it's mechanical resistance and therefore is an important parameter for scheduling interventions, especially pigging. From Fig. 6.13 it can be noted that the closer to the inlet, the faster the deposit ages. This happens due to the fact that a smaller thickness will result in a quicker increase of the wax fraction, as it can be concluded from equation 3.12. The physical explanation for faster aging rates where the deposit is thinner is that there will be a smaller volume to absorb the wax incoming through the interface, and therefore the thinner the deposit section is, the bigger the impact on wax fraction caused by a given mass flux.

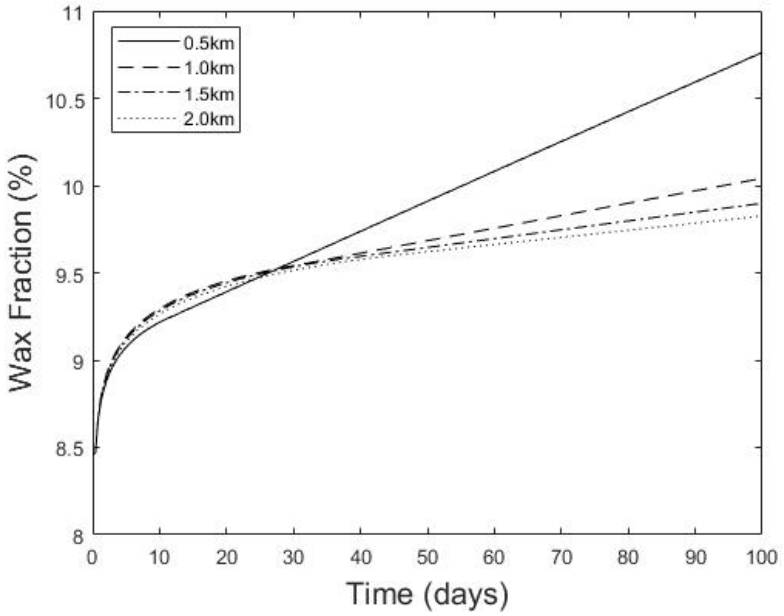

Figure 6.13: Predictions of the wax fraction of the deposit for different cross sections along the pipeline.

6.3 Wax Removal Through Electrical Heating

After the deposit has built up to its maximum thickness, the second part of the simulation starts. This part consists in removing the solid wax from the pipe walls through electrical heating of the upstream oil. To simulate the electrical resistors wrapped around the pipe, a heat flux of 300kW has been imposed with a uniform distribution along the first 200m of pipe wall. The result of this heating in the temperature field can be observed in figure 6.14. A fact worth of notice is that the hot oil remains close to the walls during the entire length of the pipe, contributing to a higher efficiency of wax removal. This occurs as a consequence of the dominance of the axial convection mechanism over the radial diffusion of heat.

The additional heat flux caused by the temperature increase in the vicinities of the deposit interface results in wax melting and subsequent thickness reduction. The progression of wax removal is displayed in figure 6.15.

6.4 Control Results

The first result to be analyzed is shown in figure 6.16. It shows the variation of pressure drop across the pipeline during the deposition an removal cycles. The increasing sections are the deposition phases and the quick decreases are caused by wax removal. It can be seen from this result that, after a while, the cycles become practically identical. More importantly, it can be noted that,

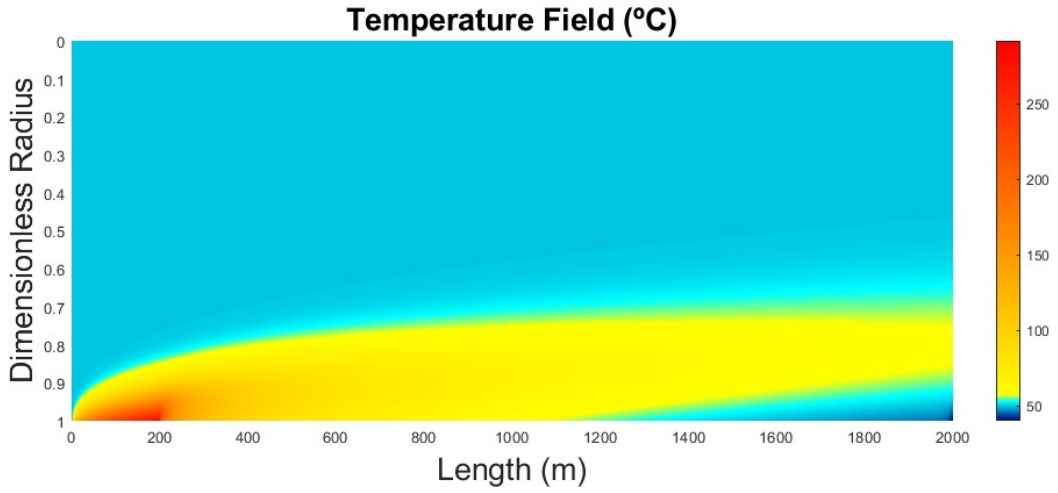

Figure 6.14: Temperature field during wax removal with electrical heating

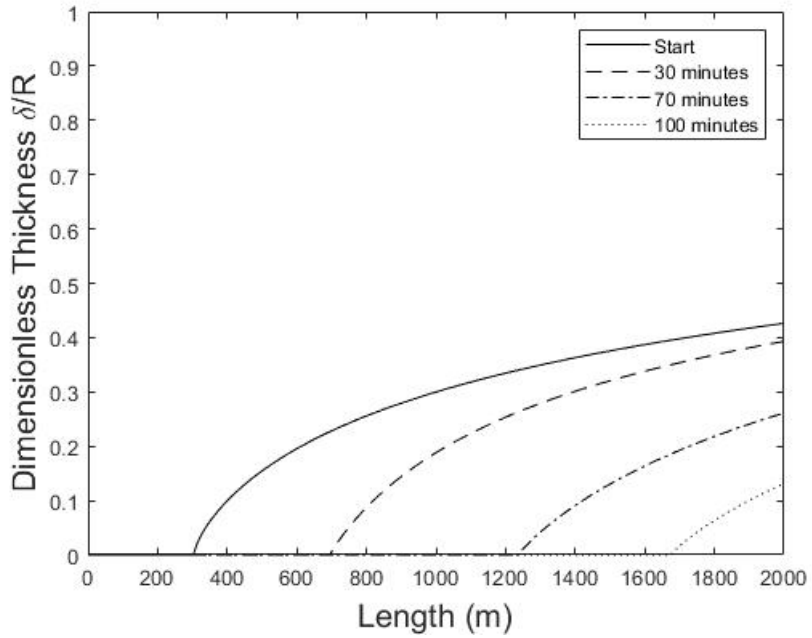

Figure 6.15: Time progression of the wax thickness profile during removal through electrical heating.

from the very beginning, two consecutive cycles present very little difference in duration. This reinforces the idea that using the history of ΔP to predict the time before the next intervention ($\mathcal{T}$) is a very good approximation, given that the oil input parameters and environmental conditions remain the same, which is usually the case.

The difference between these cycles is explained by the shape of deposit profiles. The first deposition starts with a clean pipe. After the first heating period is over, there is still some remaining wax at the end of the pipeline. The following deposition phase is then started with a residual wax deposit and reaches the limit pressure drop with a different configuration. Figure 6.17 shows

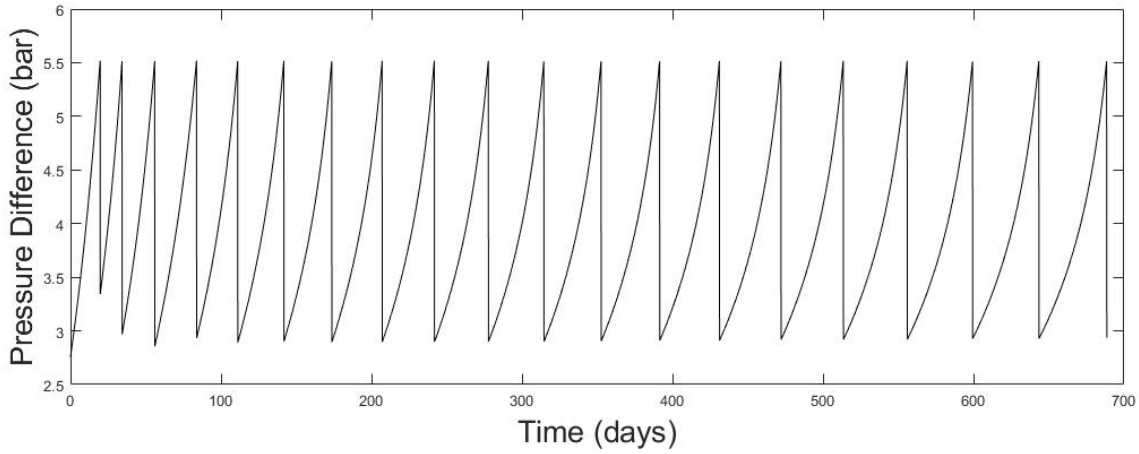

Figure 6.16: Time history of pressure difference across the pipeline during deposition and removal cycles.

a comparison between the first and last cycles of the simulation.

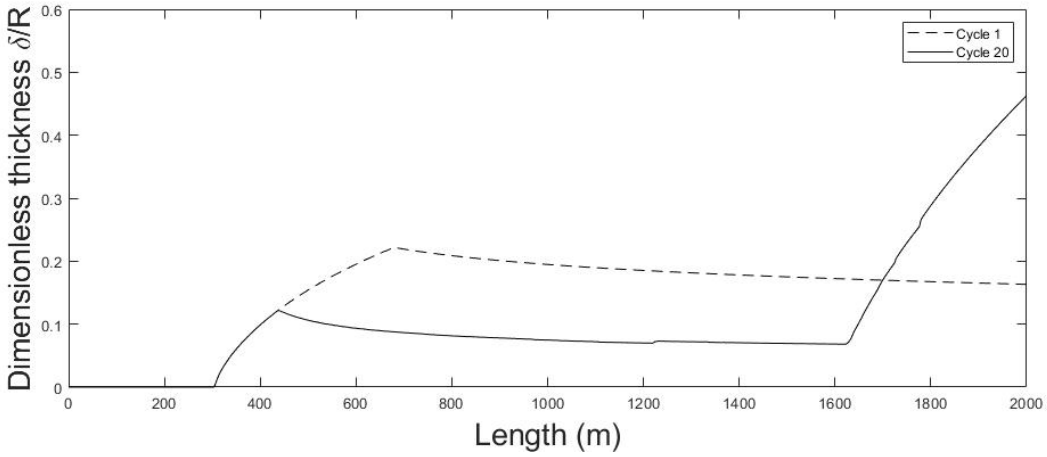

Figure 6.17: Thickness profiles comparison: First and twentieth deposition cycles.

To show that the deposition and removal cycles converge to a permanent regime, figure 6.18 exhibits the duration of the removal period for a total of 50 cycles. It can be noted that the heating time displays an asymptotic behavior. This happens as the initial condition of each heating period becomes more similar to the one found in the previous cycle.

As previously discussed in the last section of chapter 5, the objective function Π should assume a minimum value at some $t > t_{lag}$. This can be verified in figure 6.19, where the end of the lag period is marked with a dashed line.

Figure 6.20 shows how the pressure drop along the pipeline behaves when upstream oil is heated. A few hours after the heating is turned off, the pressure difference starts to rise again, as a result of a new deposition cycle.

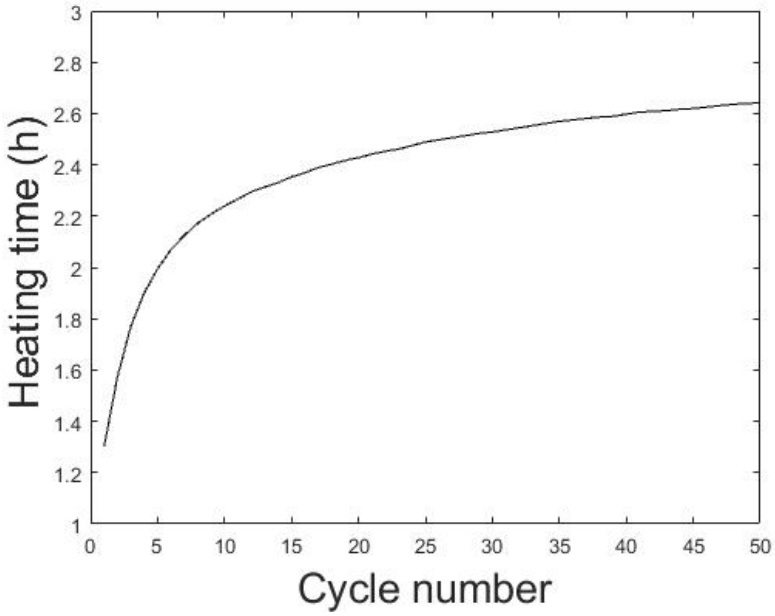

Figure 6.18: Duration of the removal phase for each cycle

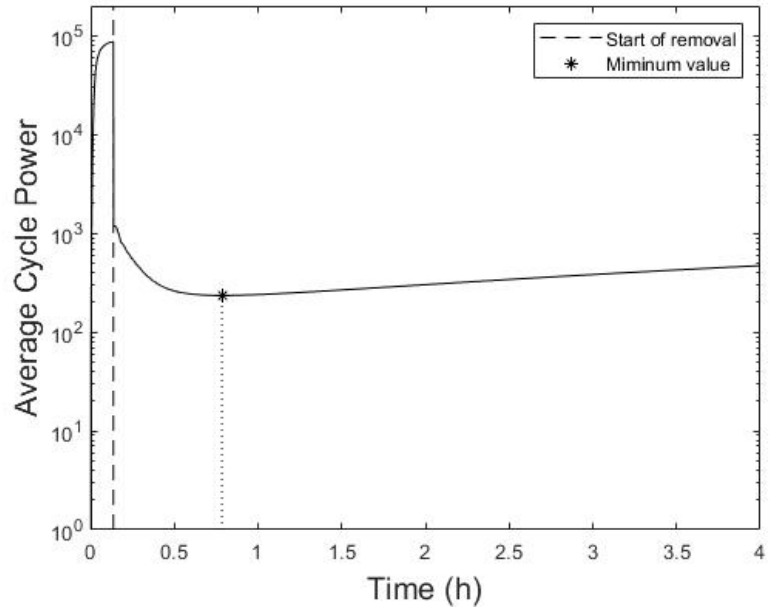

Figure 6.19: The cost function over time for continuous heating

It is also expected that the wax removal will continue for while after the heating is turned off, until all the heated oil goes through and out of the pipeline. This effect can be observed in figure 6.21, which shows the pressure drop over time during and after the heating period. The deposit takes roughly 40 minutes to stabilize after the heating is turned off. As a consequence, the cost function value decreases beyond the predicted minimum value, as $\hat{\mathcal{T}}$ continues to increase while E_c remains constant. Because of this delay, one cannot guarantee that turning of heating at the

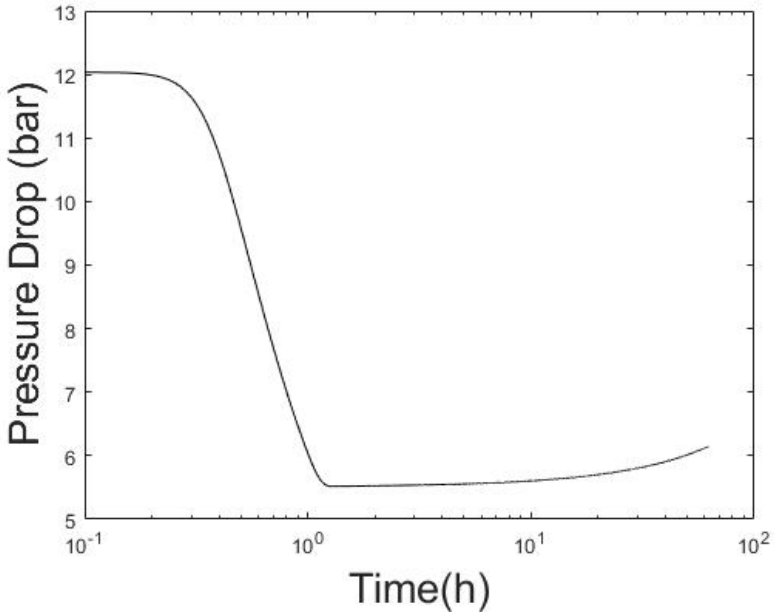

Figure 6.20: Change in pressure drop due to wax removal

minimum value of Π will ensure the optimal efficiency. An improved cost function should include a prediction of the pressure drop reduction after the deactivation of heating coils.

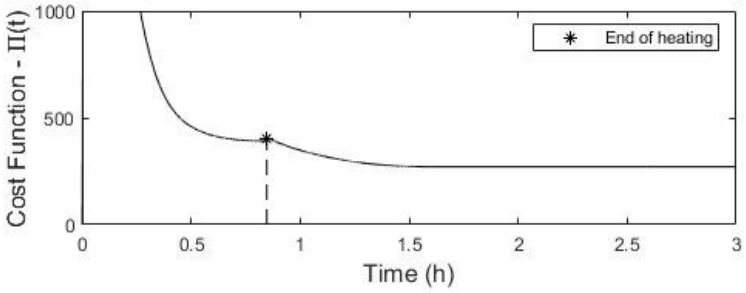

(a) Cost function - Heating turned off at minimum value.

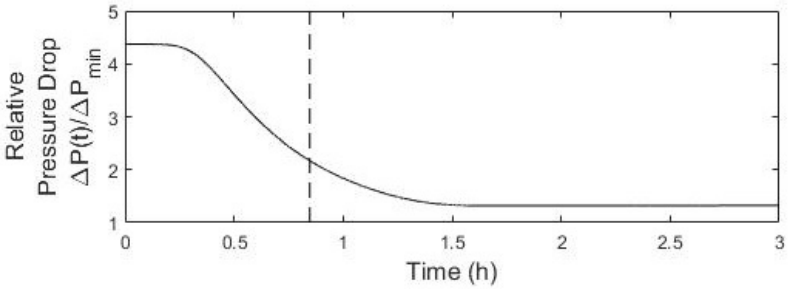

(b) Progression of the relative pressure drop over time

Figure 6.21: The effect of heating on wax removal observed through the pressure drop across the pipeline

Additionally, worth of notice is the fact that due to the restriction imposed by the wax deposi, the pressure drop may suffer severe increase. The simulations in this study were carried out considering a constant flow rate, which implies the necessity of an actively controlled pumping system. If that is the case, the pumping power would suffer an increase directly proportional to the increase in ΔP, and should, therefore, be parameter to be considered in the cost function, give that the ultimate goal of the application of such control algorithm is to minimize the overall electrical energy demand.

Chapter 7

Concluding Remarks

A wax deposition and removal model has been developed for control purposes. The model presented deposition results in good agreement with previous models available in the literature. The removal process by heating has been mathematically modelled and incorporated into the global model. In the case study considering a 2km long flow line, the electrical heating has proven to be an effective way of completely removing the wax deposit. Simulations suggest that it would be viable to remotely remove wax from short-distance oil pipelines without any aid from support vessels, divers or ROVs. A pressure down-pipe gauge(PDG) could be used to monitor the pressure drop across the line and set up a closed-loop control system to determine the time and duration of heating. In the case of very long lines, this removal technique may be used to postpone pigging interventions, which are considerably more expensive, since they require the oil production to be interrupted.

Given the fluid characteristics, pipeline dimensions and heat exchange coefficients, the present model may be used to determine the minimum necessary electrical power, as well as the number of heating stations and the distances between them, in order to guarantee the complete removal of wax. In the case of flexible pipelines, which are composed of several polymeric layers, a more specific viability study may be required to assure the integrity of all layers during the heating procedure.

A first control algorithm has been developed on the basis of a cost function that represents the mean electrical power demanded for wax removal. This function is calculated with an estimated time between removal interventions. Results have shown that calculation of the cycle duration based on the last deposition history provides a good estimation. However, it has also been verified that the pressure drop continues to decrease after the deactivation of the heating coils, and so does the cost function, as a result of the increase in the estimated cycle period. This removal lag is not negligible and should be incorporated into the cost function.

Additionally, this model was developed under the assumption of constant flow rate. In a real situation, this could be achieved through an actively controlled pumping system. If that would be

the case, because of the large difference in time-scale between the deposition and removal stages, and also because of the fact that the pumping power is directly proportional to the pressure drop, the pumping energy would most certainly be a parameter of great relevance for determining the periodicity of heating cycles.

7.1 Future Works

- **Pumping Power**: In a controlled flow rate system, the increase in pumping power due to the presence of wax deposit should be incorporated into the cost function to allow the minimization of the overall electrical power demand.
- **Long exportation lines**: Development of a viability study for wax removal in very long oil pipelines with the use of several heating stations.
- **Boundary condition for heat transfer in transient regimes**: The boundary condition for heat exchange with the environment used in this work was based on the heat resistance theory, which is valid for permanent regime. During the deposition phase, this assumption is valid, whereas during removal phase, the temperature field changes quickly inside the deposit, pipe wall and insulation layers and must be calculated in order to allow for an accurate prediction of the heat loss to the environment.
- **Turbulent regimes:** The present model has been developed for laminar flows. Oil flows in production and exportation lines are often turbulent. An upgraded model should include a turbulent velocity profile as well as turbulent thermal and mass diffusivities.
- **Dynamic Flow:** Development of a computational fluid dynamics model coupled to the deposition model in order to enable the oil flow to adapt to the constantly changing geometry of the wax deposit.
- **Variable Viscosity:** Implementation of oil viscosity as a function of temperature, wax concentration and shear rate.
- **Multi-phase flows:** The petroleum that comes out of reservoirs usually contains high fractions of other fluids such as water and gas. A multi-phase flow model would contribute towards the development of a robust simulation tool for all kinds of situations encountered in the field.

BIBLIOGRAPHIC REFERENCES

[1] [Online]. Available: https://torp.ku.edu/wax-deposition

[2] [Online]. Available: https://www.london-nano.com/research/asphaltene-aggregation-presence-laponite-clay

[3] Y. A. Çengel and A. J. Ghajar, *Heat and Mass Transfer Fundamentals and Applications*, 5th ed. McGraw Hill Education, 2015.

[4] Z. Huang, H. S. Lee, M. Senra, and H. S. Fogler, "A fundamental model of wax deposition in subsea oil pipelines," *AIChE Journal*, vol. 57, no. 11, Feb. 2011.

[5] P. Singh, R. Venkatesan, H. S. Fogler, and N. Nagarajan, "Formation and aging of incipient thin film wax-oil gels," *AIChE Journal*, vol. 46, no. 5, May 2000.

[6] S. Misra, S. Baruah, and K. Singh, "Paraffin problems in crude oil production and transportation: A review," *SPE Production & Facilities*, vol. 10, 1995.

[7] L. F. A. Azevedo and A. M. Teixeira, "A critical review of the modeling of wax deposition mechanisms," *PETROLEUM SCIENCE AND TECHNOLOGY*, vol. 21, no. 3 and 4, pp. 393–408, 2003.

[8] M. C. K. D. Oliveira, R. M. Carvalho, A. B. Carvalho, B. C. Couto, F. R. D. Faria, and R. L. P. Cardoso, "Waxy crude oil emulsion gel: Impact on flow assurance," *Energy & Fuels*, vol. 24, 2010.

[9] H. S. F. Zhenyu Huang, Sheng Zheng, *Wax Deposition Experimental Characterizations, Theoretical Modeling, and Field Practices*, A. Y. Dandekar, Ed. CRC Press, 2015.

[10] Y. Chi, N. Daraboina, and C. Sarica, "Effect of the flow field on the wax deposition and performance of wax inhibitors: Cold finger and flow loop testing," *Energy and Fuels*, 2017.

[11] M. Al-Yaari, "Paraffin wax deposition: Mitigation & removal techniques," in *SPE Saudi Arabia section Young Professionals Techical Symposium*, 2011.

[12] R. C. Sarmento, G. A. S. Ribbe, and L. F. A. Azevedo, "Wax blockage removal by inductive heating of subsea pipelines," *Heat Transfer Engineering*, 2004.

[13] N. Wang, M. Prodanović, and H. Daigle, "Nanopaint application for flow assurance with electromagnetic pig," *Journal of Petroleum Science and Engineering*, 2019.

[14] V. A. Balakirev, G. V. Sotnikov, Y. V. Tkach, and T. Y. Yatsenko, "Removal of asphalt–paraffin deposits in oil pipelines by a moving source of high-frequency electromagnetic radiation," *Journal of Technical Physics*, vol. 46, no. 9, pp. 1069–1075, 2001.

[15] E. B. Hunt, "Laboratory study of paraffin deposition," *SPE Journal of Petroleum Technology*, vol. 14, pp. 1259–1269, 1962.

[16] E. Burger, T. Perkins, and J. Striegler, "Studies of wax deposition in the trans alaska pipeline," *Journal of Petroleum Technology*, vol. 33, pp. 1075–1086, 1981.

[17] A. Leiroz and L. Azevedo, "Studies on the mechanisms of wax deposition in pipelines," in *Offshore Technology Conference*, 2005.

[18] A. S. Nazar, B. Dabir, H. Vaziri, and M. Islam, "Experimental and mathematical modeling of wax deposition and propagation in pipes transporting crude oil," *Energy Sources*, vol. 27, pp. 185–207, 2005.

[19] S. Correra, A. Fasano, L. Fusi, and D. Merino-Garcia, "Calculating deposit formation in the pipelining of waxy crude oils," *Meccanica*, vol. 42, pp. 149–165, 2007.

[20] P. Singh, H. S. Fogler, and N. Nagarajan, "Prediction of the wax content of the incipient wax-oil gel in a pipeline: An application of the controlled-stress rheometer," *Journal of Rheology*, vol. 43, p. 1437, 1999.

[21] A. Majeed, B. Bringedal, and S. Overa, "Model calculates wax deposition for n. sea oils," *Oil & Gas Journal*, vol. 88, pp. 63–69, 1990.

[22] R. E. Hampton, A. A. Mammoli, A. L. Graham, and N. Tetlow, "Migration of particles undergoing pressure-driven flow in a circular conduit," *Journal of Rheology*, vol. 41, p. 621, 1997.

[23] N. Tetlow and A. L. Graham, "Particle migration in a couette apparatus: Experiment and modeling," *Journal of Rheology*, vol. 42, p. 307, 1998.

[24] G. Segré and A. Silberberg, "Behaviour of macroscopic rigid spheres in poiseuille flow part 1. determination of local concentration by statistical analysis of particle passages through crossed light beams," *Journal of Fluid Mechanics*, vol. 14, no. 1, p. 115, 1962.

[25] J. Creek, H. J. Lund, J. P. Brill, and M. Volk, "Wax deposition in single phase flow," *Fluid Phase Equilibria*, vol. 158–160, p. 801:811, 1999.

[26] B. Edmonds, T. Moorwood, R. Szczepanski, and X. Zhang, "Simulating wax deposition in pipelines for flow assurance," *Energy & Fuels*, vol. 22, pp. 729–741, 2008.

[27] M. S. A. A. Matzain, H.-Q. Zhang, M. Volk, J. P. Bril, and J. L. Creek, "Investigation of paraffin deposition during multiphase flow in pipelines and wellbores—part 2: Modeling," *JOURNAL OF ENERGY RESOURCES TECHNOLOGY - TRANSACTIONS OF THE ASME*, vol. 123, no. 2, pp. 150–157, Jun. 2001.

[28] K. Paso, M. Senra, Y. Yi, A. M. Sastry, and H. S. Fogler, "Paraffin polydispersity facilitates mechanical gelation," *Industrial & Engineering Chemistry Research*, vol. 44, no. 18, pp. 7242–7254, 2005.

[29] A. Aiyejina, D. P. Chakrabarti, A. Pilgrim, and M. Sastry, "Wax formation in oil pipelines: A critical review," *International Journal of Multiphase Flow*, vol. 37, pp. 671–694, 2011.

[30] V. R., "The deposition and rheology of organic gels," Ph.D. dissertation, Dept. of Chemical Engineering, University of Michigan, 2004.

[31] S. P., V. R., F. H.S., and N. N.R., "Morphological evolution of thick wax deposits during aging," *AIChE Journal*, 2001.

[32] Z. Huang, "Application of the fundamentals of heat and mass transfer to the investigation of wax deposition in subsea pipelines," Ph.D. dissertation, University of Michigan, 2011.

[33] W. Hayduk and B. S. Minhas, "Correlations for prediction of molecular diffusivities in liquids," *The Canadian Journal of Chemical Engineering*, vol. 60, Apr. 1982.

[34] S. Zheng, M. Saidoun, T. Palermo, K. Mateen, and H. S. Fogler, "Wax deposition modeling with considerations of non-newtonian characteristics: Application on field-scale pipeline," *Energy Fuels*, 2017.

[35] H. S. Lee, "Computational and rheological study of wax deposition and gelation in subsea pipelines," PhD thesis, University of Michigan, Ann Arbor, Michigan, 2008.

[36] G. M. Villazon and F. Civan, "Modeling multiphase wax deposition in submarine pipelines after shut-in," in *SPE 124725*. Society of Petroleum Engineers, 2009.